Supplementary Material For

Molecular insight into hydrogen storage in clathrate hydrates: The effect of different promoters on the spontaneous nucleation of hydrogen hydrates studied via microsecond-scale molecular dynamics simulations

Fengyi Mi[†,‡], Fulong Ning[*,†], Thijs J.H. Vlugt[‡], Othonas A. Moultos[*,‡]

[†]National Center for International Research on Deep Earth Drilling and Resource Development, Faculty of Engineering, China University of Geosciences, Wuhan, Hubei 430074, China

[‡]Engineering Thermodynamics, Process & Energy Department, Faculty of Mechanical Engineering, Delft University of Technology, Leeghwaterstraat 39, Delft, 2628CB, the Netherlands

[*]Authors to whom correspondence should be addressed. nflzx@cug.edu.cn, o.moultos@tudelft.nl

Contents of the Supplementary Material

S1. Simulation details S5

Fig. S1. The molecular structures of the six promoter molecules, *i.e.,* CH_4, CO_2, C_2H_6, C_3H_8, C_5H_{10}, and THF molecules, in this study S6

Table S1. System sizes of the seven different systems. S6

Table S2. Pressure-temperature equilibrium conditions for hydrate dissociation. S6

Table S3. The force field parameters for H_2O, H_2, and promoter molecules in the system. S7

Table S4. The force field parameters for promoter molecules in the system. S8

Fig. S2. The schematic diagram of the initial configurations for the homogeneous and two-phase model. S9

S2. Calculation of properties **S10**

S2.1. Gibbs free energies of various promoters in water S10

S2.2. Average diffusion coefficient (K_{DC}) S10

S2.3. Gas mole fraction S10

S2.4. Residence time correlation function S10

S2.5. Induction time S11

S2.6. H_2 storage capacity S11

S3. Supporting Figures **S12**

Fig. S3. Time evolution of the number of hydrogen bonds near promoter molecules in different repeated systems S12

Fig. S4. Time evolution of the diffusion coefficient for H_2 molecules in bubble and solution in different repeated systems S12

Fig. S5. Time evolution of the diffusion coefficient for promoter molecules in bubble and solution in different repeated systems S13

Fig. S6. Time evolution of the average residence time for H_2O molecules near promoter molecules in different repeated systems S13

Fig. S7. Evolution of probability distribution of the distances between H_2 in water and various promoter molecules in different systems S14

Fig. S8. Probability distribution of the distances between H_2 in water and various promoter molecules in different repeated systems S14

Fig. S9. Time evolution of the number of H_2 and CH_4 molecules adsorbed to each H_2-occupied and CH_4-occupied cage-faces for the H_{CH_4} repeated systems S15

Fig. S10. Time evolution of the number of H_2 and CO_2 molecules adsorbed to each H_2-occupied and CO_2-

occupied cage-faces for the H_{CO_2} repeated systems S15

Fig. S11. Time evolution of the number of H_2 and C_2H_6 molecules adsorbed to each H_2-occupied and C_2H_6-occupied cage-faces for the $H_{C_2H_6}$ repeated systems S16

Fig. S12. Time evolution of the number of H_2 and THF molecules adsorbed to each H_2-occupied and THF-occupied cage-faces for the H_{THF} repeated systems S16

Fig. S13. Correlation plot of the number of gas molecules adsorbed cage-faces and dissolved in water for different systems S17

Fig. S14. Time evolution of (a) gas mole fraction x_{gas} in water and (b) the number of promoter molecules in water/hydrate for different systems S17

Fig. S15. Simulation snapshots of binary H_2 hydrates formed at the end of the simulation (at the 3.0 μs) in the different systems: (a) H_{Pure}, (b) H_{CH_4}, (c) H_{CO_2}, (d) $H_{C_2H_6}$, (e) $H_{C_3H_8}$, and (f) $H_{C_5H_{10}}$. S18

Fig. S16. Time evolution of the number of water molecules in hydrate and solution for the H_{CH_4} repeated systems S19

Fig. S17. Time evolution of the number of water molecules in hydrate and solution for the H_{CO_2} repeated systems S20

Fig. S18. Time evolution of the number of water molecules in hydrate and solution for the $H_{C_2H_6}$ repeated systems S20

Fig. S19. Time evolution of the number of water molecules in hydrate and solution for the H_{THF} repeated systems S21

Fig. S20. Time evolution of F_4 order parameters within 0.35 nm of H_2 and promoter molecules in the four repeated simulations (Run1 - Run4) for the different systems S22

Fig. S21. Time evolution of F_4 order parameters within 0.35 nm of H_2 and promoter molecules in the four repeated simulations (Run1 - Run4) for the different systems S23

Fig. S22. Time evolution of the number of H_2-occupied cages in the four repeated simulations (Run1 - Run4) for the different systems S24

Fig. S23. Time evolution of the number of promoter-occupied cages in the four repeated simulations (Run1 - Run4) for the different systems S25

Fig. S24. Time evolution of the number of H_2-occupied cages in different systems S26

Fig. S25. Time evolution of the number of promoter-occupied cages in different systems S26

Fig. S26. Time evolution of the number of multi-occupied cages in different systems S27

Fig. S27. Time evolution of F_4 order parameters for different systems S27

Fig. S28. Time evolution of the number of H_2 storage in hydrates for the seven systems S28

Fig. S29. Time evolution of the number of H_2 molecules in nanobubble for different systems S28

Fig. S30. Time evolution of the number of hydrate cages for the seven systems S29

S4. Supporting Videos **S30**

Video S1. Spontaneous nucleation processes of pure H_2 hydrates from two-phase solutions for the H_{Pure} system S30

Video S2. Spontaneous nucleation processes of binary H_2-CH_4 hydrates from two-phase solutions for the H_{CH_4} system S30

Video S3. Spontaneous nucleation processes of binary H_2-CO_2 hydrates from two-phase solutions for the H_{CO_2} system S30

Video S4. Spontaneous nucleation processes of binary H_2-C_2H_6 hydrates from two-phase solutions for the $H_{C_2H_6}$ system S30

Video S5. Spontaneous nucleation processes of binary H_2-C_3H_8 hydrates from two-phase solutions for the $H_{C_3H_8}$ system S30

Video S6. Spontaneous nucleation processes of binary H_2-C_5H_{10} hydrates from two-phase solutions for the $H_{C_5H_{10}}$ system S30

Video S7. Spontaneous nucleation processes of binary H_2-THF hydrates from two-phase solutions for the H_{THF} system S30

References **S31**

S1. Simulation details

Common promoters, such as CH_4, CO_2, C_2H_6, C_3H_8, C_5H_{10}, and THF molecules, were studied, and their molecular structures are shown in Fig. S1. The systems were uniformly composed of H_2, H_2O, and promoter molecules. A system of pure H_2 was also studied as a reference. The decision to use pure H_2 hydrates as a reference for evaluating the promoting effect was based on the primary goal of this study: to explore how these molecules influence the formation of binary H_2 hydrates. The differences in nucleation rates and mechanisms are mainly attributed to the specific interactions between H_2, water, and the respective promoter molecules, which is a key focus of our work. The system sizes are listed in Table S1. These molecules were all randomly inserted into the box. The H_2 to promoter molecule ratio of 0.625 was chosen based on previous studies for optimal binary hydrate formation [1]. The number ratio of promoter molecules to H_2O molecules is 17, which is consistent with the ratio of large cages to H_2O molecules in a standard SII-type hydrate structure. The detailed force field parameters for H_2O, H_2, and promoter molecules in the system are provided in Tables S2 and S3. Binary hydrates nucleated from the gas-liquid two-phase in all systems. The gas-liquid two-phase configuration was obtained by simulating a homogeneous solution mixture at 300 K and 100 bar (Fig. S2(a-h)). Conditions set at 300 K and 100 bar can accelerate phase separation, as shown in previous MD studies [2]. First, all molecules were randomly inserted into a box ($5.2 \times 5 \times 5$ nm^3) to form a homogeneous solution mixture. Subsequently, a 30-ns simulation was performed under the *NPT* ensemble. The gas-liquid two-phase configuration forms spontaneously in the simulation box. The 30-ns simulation time is long enough to ensure that most gas molecules form nanobubbles rather than dissolve in water. Temperature and pressure during equilibration were controlled using the velocity-rescaling thermostat [3] with a time constant of 0.1 and the Berendsen barostat [4] with a time constant of 1 ps, respectively.

The equations of motion were integrated according to the leapfrog algorithm with a 2.0 fs timestep. The well depth $\varepsilon_{O(CO_2)\text{-}O(H_2O)}$ between the oxygen in CO_2 and the oxygen in H_2O was scaled by a factor of 1.08. The initial configurations were energy minimized using the steepest descent algorithm. A 2-ns simulation was performed to equilibrate the simulation system at 240 K and 1100 bar using the velocity-rescaling thermostat [3] and Berendsen barostat [4]. Then, a production run for 3.0 μs was performed under the *NPT* ensemble at 240 K and 1100 bar to investigate the nucleation of binary H_2 hydrate. The temperature and pressure were maintained using the Nosé-Hoover thermostat [5] and Parrinello-Rahman barostat [6] with time constants of 2 ps and 4 ps, respectively. The cut-off radius for computing the Van der Waals forces was set to 1.0 nm. For electrostatic energy computation, the particle-mesh Ewald [7] algorithm was used with the cut-off as 1.0 nm and Fourier grid spacing of 0.12 nm. Trajectories are saved every 10 ps. Periodic boundary conditions were applied in all directions. To monitor the nucleation of binary hydrate, the cage analysis algorithm proposed by Jacobson *et al.* [8] was used to display the seven cage types (5^{12}, $5^{12}6^2$, $5^{12}6^3$, $5^{12}6^4$, $4^15^{10}6^2$, $4^15^{10}6^3$, and $4^15^{10}6^4$).

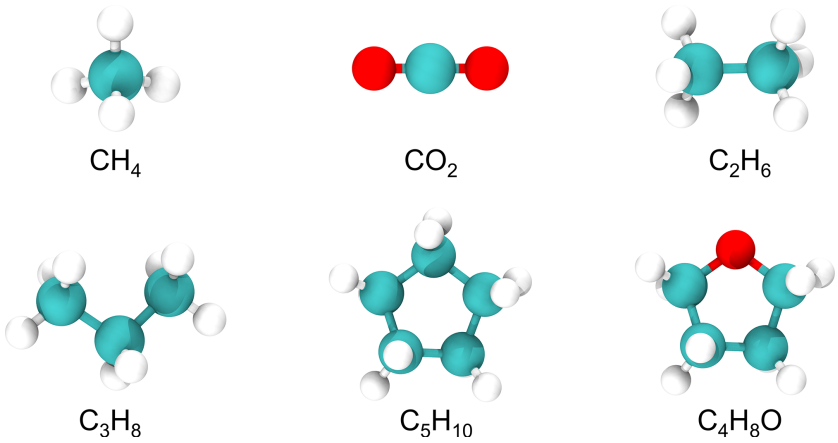

Fig. S1. Molecular structures of the six promoter molecules, *i.e.,* CH_4, CO_2, C_2H_6, C_3H_8, C_5H_{10}, and THF molecules, in this study.

Table S1. System sizes of the seven different systems.

	Systems: 240 K/1100 bar			
System	$N_{promoter}$	N_{H_2}	N_{H_2O}	Time
H_{Pure}	0	300	3060	3.0 μs
H_{CH_4}	180	300	3060	3.0 μs
H_{CO_2}	180	300	3060	3.0 μs
$H_{C_2H_6}$	180	300	3060	3.0 μs
$H_{C_3H_8}$	180	300	3060	3.0 μs
$H_{C_5H_{10}}$	180	300	3060	3.0 μs
H_{THF}	180	300	3060	3.0 μs

Table S2. Pressure-temperature equilibrium conditions for hydrate dissociation.

	Pressure – temperature equilibrium conditions for hydrate dissociation		
Species	Melting Temperature/[K]	Pressure/[MPa]	References
CH_4	225.4	0.46	[9]
CO_2	247.1	0.4066	[10]
C_2H_6	269.3	0.441	[11]
C_3H_8	277.2	0.405	[12]
C_5H_{10}	276.4	0.11	[13]
THF	277.5	0.11	[14]

Table S3. Force field parameters for TIP4P/ice [15], Alavi *et al.* H_2 [16], and TraPPE CO_2 [17]. σ and ε are the Lennard-Jones parameters, in units of nm and kJ/mol, respectively; q is the partial charge in units of elementary charge (e); m is the atomic mass in units of g/mol.

atom	ε / [kJ/mol]	σ / [nm]	q / [e]	m / [g/mol]
H_2O				
O (MW)	0	0	-1.1794	0
O	0.8822	0.31668	0	16
H	0	0	0.5897	1.008
H_2				
Hh	0	0	0.4932	1.008
Hm	0.2852	0.3083	-0.9864	0
CO_2				
C	0.224478	0.28	0.70	12.011
O	0.656806	0.305	-0.35	15.9994
O (OM)	0	0	0	0

According to the Laplace equation, the curvature of a gas-liquid interface (i.e., bubble size) results in a pressure difference across the interface. This pressure difference can influence the local concentration of guest molecules in the liquid phase, thereby affecting the driving force for hydrate nucleation. In our simulations, our systems are relatively small, and although different runs produced some variations in bubble size, the overall statistical analysis of nucleation events showed similar trends across the replicas. Interfacial tension is a crucial factor and variations in bubble curvature can lead to differences in guest concentration locally. Based on the Laplace equation, smaller bubbles have higher internal pressure compared to larger gas layers, which can increase the local solubility of H_2. These variations could influence the local chemical potential and, consequently, the nucleation kinetics. Although our simulation box is small and the variations in bubble sizes are somewhat limited by the system size, we should note that even small differences may have an impact on local concentrations. Our four-replica simulation protocol indicates that, on average, the nucleation kinetics remain consistent; however, we now note that interfacial tension is a contributing factor that warrants further quantitative investigation. Future studies, using much larger system size, could focus on quantifying the size distribution of gas bubbles and directly correlate these measurements with local H_2 concentrations. This will allow for a more detailed exploration of how interfacial phenomena influence hydrate nucleation.

Table S4. Parameters for the OPLS-AA force field [18] for the five promoter molecules. σ and ε are the Lennard-Jones parameters, in units of nm and kJ/mol, respectively; q is the partial charge in units of elementary charge (e); m is the atomic mass in units of g/mol.

atom	ε / [kJ/mol]	σ / [nm]	q / [e]	m / [g/mol]
CH_4				
C(CT)	0.276144	0.35	-0.24	12.011
H (HC)	0.12552	0.25	0.06	1.008
C_2H_6				
C(CT)	0.276144	0.35	-0.18	12.011
H (HC)	0.12552	0.25	0.06	1.008
C_3H_8				
C(CT1)	0.276144	0.35	-0.12	12.011
C(CT2)	0.276144	0.35	-0.18	12.011
H (HC)	0.12552	0.25	0.06	1.008
C_5H_{10}				
C(CT)	0.276144	0.35	-0.12	12.011
H (HC)	0.12552	0.25	0.06	1.008
THF				
C(CT)	0.276144	0.35	-0.12	12.011
C(CT1)	0.276144	0.35	0.14	12.011
O(OS)	0.58576	0.29	-0.4	15.9994
H (HL)	0.12552	0.25	0.03	1.008
H (HC)	0.12552	0.25	0.06	1.008

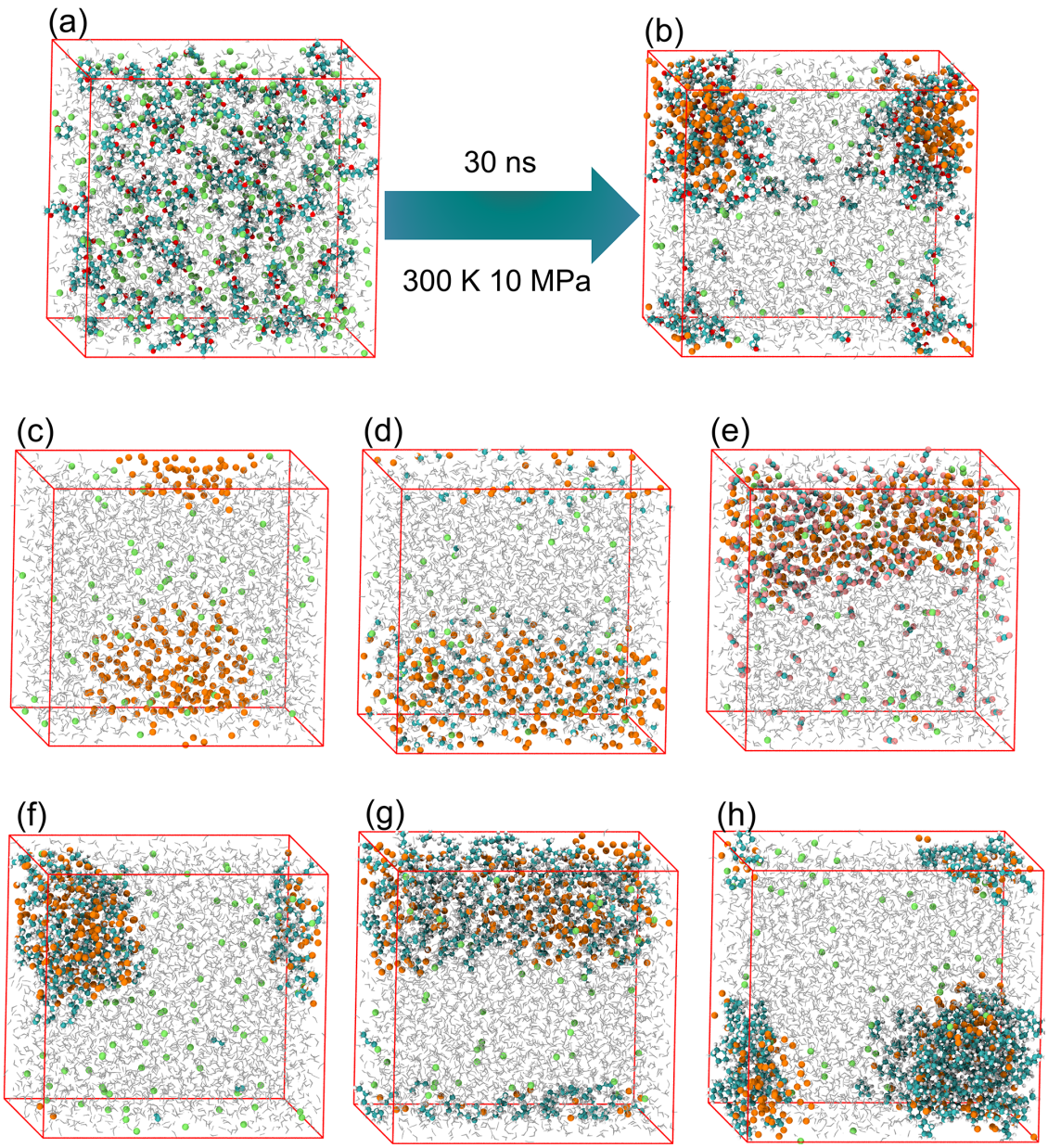

Fig. S2. Simulation snapshots of the (a) initial configuration for the homogeneous solution. The snapshots of two-phase models at 0 μs in different seven systems, *i.e.*, (b) H_{THF}, (c) H_{Pure}, (d) H_{CH_4}, (e) H_{CO_2}, (f) $H_{C_2H_6}$, (g) $H_{C_3H_8}$, and (h) $H_{C_5H_{10}}$. Promoter molecules are displayed as cyan (C atom), red (O atom), and white (H atom). Orange balls, green balls, and silver lines represent H_2 in nanobubble, H_2 in solution, and H_2O molecules, respectively.

S2. Calculation of properties

S2.1. Gibbs free energies of various promoters in water

The Gibbs free energies of various promoters in water are calculated by the GROMACS 2022 [19]. A single promoter molecule (*i.e.*, CH_4, CO_2, C_2H_6, C_3H_8, C_5H_{10}, and THF molecules) was placed in the center of a box of size 3.2 × 3.2 × 3.2 nm^3. Then 800 water molecules were randomly placed into the box to form the initial configuration. The charge of each promoter molecule was set to 0 to avoid electrostatic interactions. The simulation process was as follows: energy minimization - 100 ps *NVT* equilibrium - 100 ps *NPT* equilibrium - 1 ns production simulation. The option gmx_bar in the post-processing of GROMACS was used to analyze the data of simulation.

S2.2. Average diffusion coefficient (K_{DC})

The centre of mass mean square displacements (MSD) and diffusion coefficients K_{DC} are calculated using the option *gmx_mpi msd* in the post-processing of GROMACS 2022 [19]. An index file containing atom numbers of H_2, CH_4, CO_2, C_2H_6, C_3H_8, C_5H_{10}, and THF molecules in water and in nanobubble is used and the MSD is averaged over these atoms. In this study, each centre of mass MSD is calculated within 1 ns for H_2, CH_4, CO_2, C_2H_6, C_3H_8, C_5H_{10}, and THF molecules in water and in nanobubble. Therefore, each diffusion coefficient is the average value within intervals of 1 ns.

S2.3. Gas mole fraction

We use VMD software [20] to determine the state of gas molecules (H_2 and promoter molecules) or water molecules. At each frame, we check each gas molecule to find the number of water molecules and other gas molecules surrounding it (within a certain cutoff). This method is used to determine whether each gas molecule belongs to the water phase or nanobubbles. The gas mole fraction in the aqueous phase is defined as the number of gas molecules in the aqueous phase divided by the number of water and gas molecules in the aqueous phase, as follows

$$gas\ mole\ fraction = \frac{N_{gas}}{N_{gas} + N_{water}} \tag{2}$$

where N_{gas} is the number of gas molecules (H_2 and promoter molecules) in the aqueous phase. N_{water} is the number of water molecules. It is noted that water molecules in hydrates are excluded.

S2.4. Residence time correlation function

The principle of correlation functions is well established and documented in GROMACS 2022 [19]. The residence time correlation function is one such function. The definition of the residence correlation function $C_f(t)$ for residence $f(t)$ is:

$$C_f(t) = \langle f(\xi) f(\xi + t) \rangle_\xi \tag{3}$$

$\langle\ \rangle$ indicates averaging over ξ, that is over time origins. The residence time τ is calculated by the numeric integration of the residence correlation function:

$$\tau = \int_0^\infty C_f(t)dt \tag{4}$$

In practical MD simulation, correlation functions are calculated based on data points with discrete time intervals Δt, so the residence correlation function $C_f(t)$ is:

$$C_f(j\Delta t) = \frac{1}{N-j}\sum_{i=0}^{N-1-j} f(i\Delta t)f((i+j)\Delta t) \tag{5}$$

where N is the number of available time frames for the calculation. In this study, each residence time τ_{Res} is calculated within 1 ns for H_2O molecules near CH_4, CO_2, C_2H_6, C_3H_8, C_5H_{10}, and THF molecules in water. The GROMACS command *gmx_mpi hbond -ac -contact* can perform the calculation of the residence correlation function.

S2.5. Induction time

To monitor binary H_2 hydrate nucleation, the induction time is defined. The F_4 order parameter serves as an effective discriminator for distinguishing the water phase, with average values of -0.04, -0.4, and 0.7 for liquid water, ice, and hydrate, respectively[21]. The F_4 order parameter is defined by

$$F_4 = \langle cos(3\emptyset)\rangle \tag{6}$$

The F_4 is computed by the water-water pair as a function of the torsional angle $\emptyset$ between oxygen atoms within 3.5 Å and the outermost hydrogen atoms in the water-water pairs. The induction time is the time at which the F_4 value is 0.05.

S2.6. H_2 storage capacity

During the period of 0 - 3.0 μs, H_2 molecules have two states, *i.e.*, in hydrate or non-hydrate. H_2 storage capacity (%) is defined as the number of H_2 molecules stored in hydrate divided by the total number of H_2 molecules.

$$Capacity = \frac{N_{H2-hydrate}}{N_{H2-total}} \times 100\% \tag{7}$$

where $N_{H2-hydrate}$ is the number of H_2 molecules stored in hydrate cages, $N_{H2-total}$ is the number of H_2 molecules in the system, *i.e.,* 300 molecules. In this study, the percentage of H_2 storage is calculated to average the last 0.1 μs.

S3. Supporting Figures

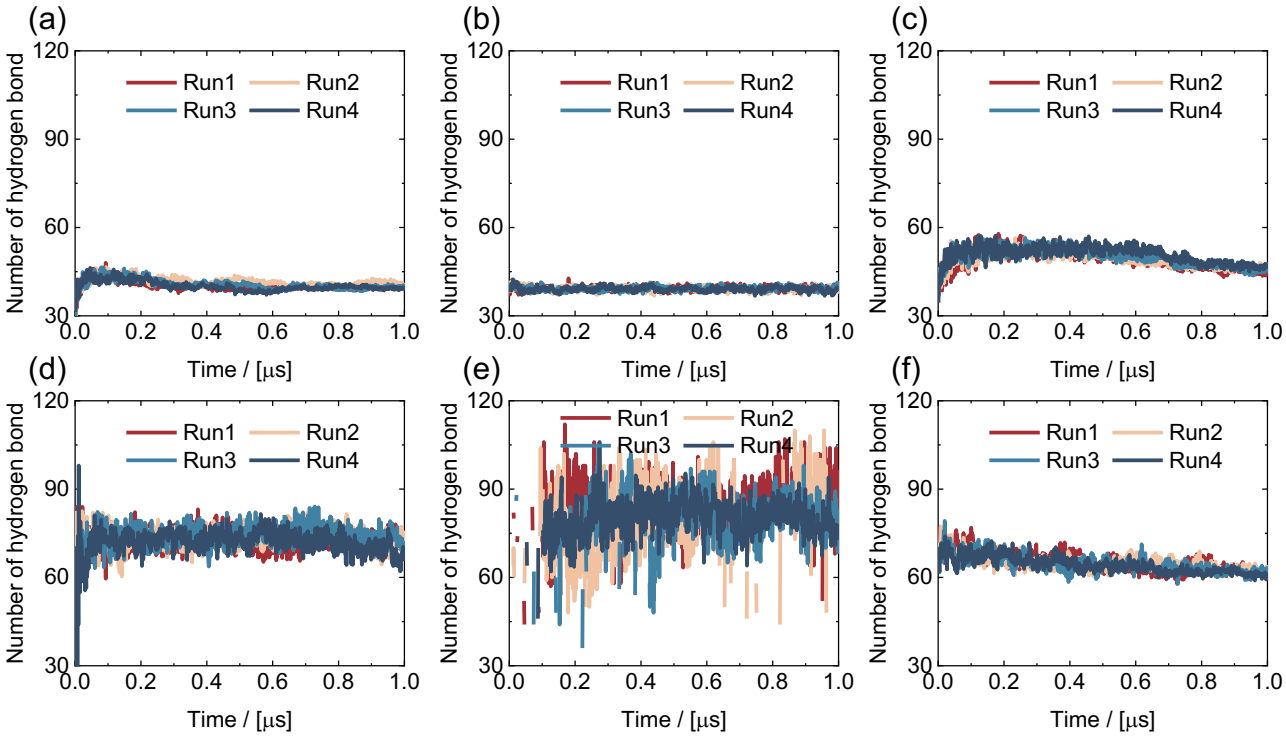

Fig. S3. Time evolution of the number of hydrogen bonds near promoter molecules in different repeated systems, *i.e.*, (a) H_{CH_4}, (b) H_{CO_2}, (c) $H_{C_2H_6}$, (d) $H_{C_3H_8}$, (e) $H_{C_5H_{10}}$, and (f) H_{THF}.

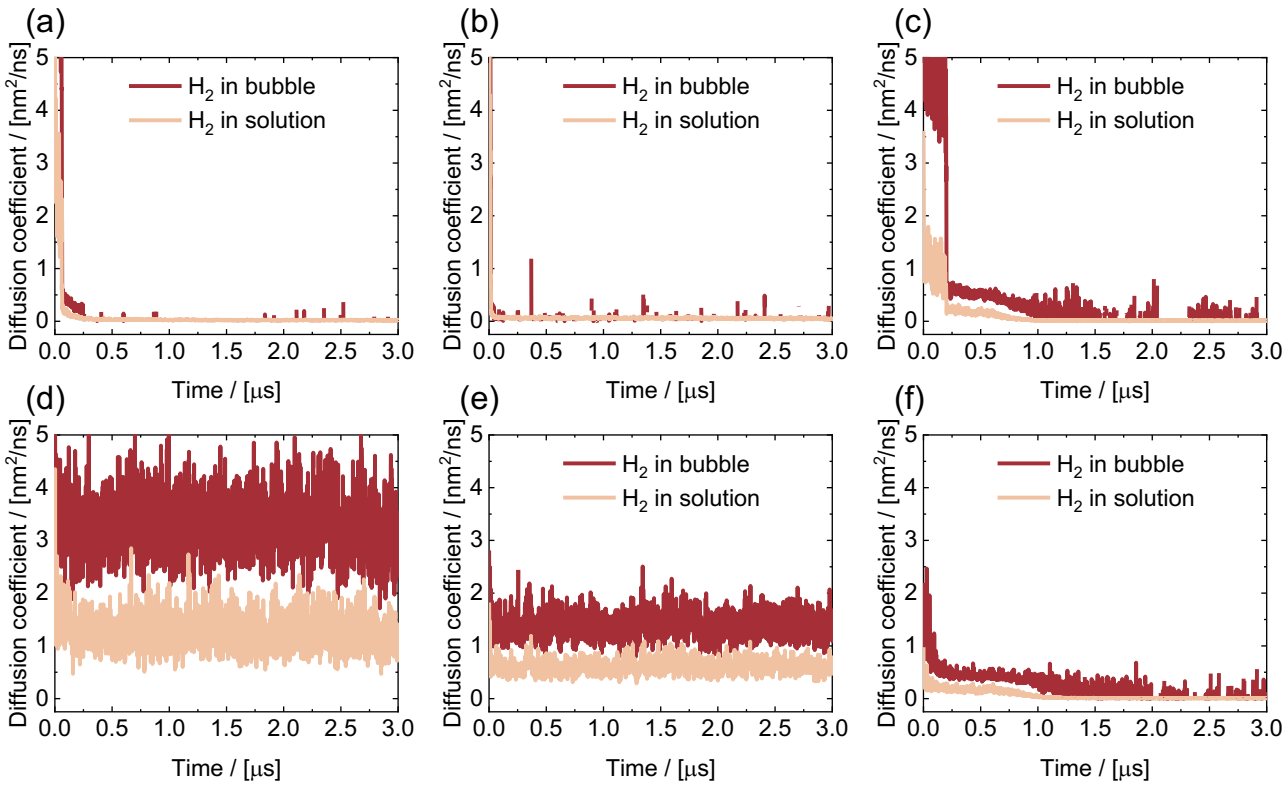

Fig. S4. Time evolution of the diffusion coefficient for H_2 molecules in bubble and solution in different repeated systems, *i.e.*, (a) H_{CH_4}, (b) H_{CO_2}, (c) $H_{C_2H_6}$, (d) $H_{C_3H_8}$, (e) $H_{C_5H_{10}}$, and (f) H_{THF}.

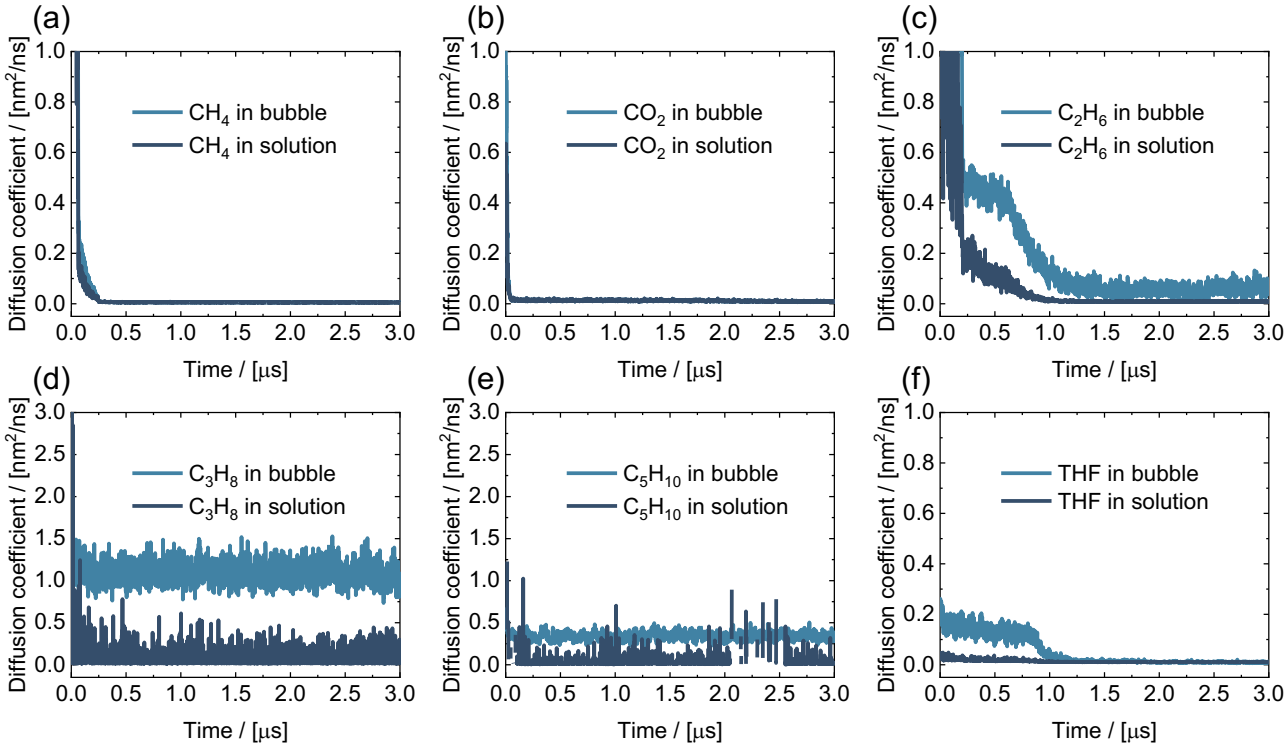

Fig. S5. Time evolution of the diffusion coefficient for promoter molecules in bubble and solution in different repeated systems, *i.e.*, (a) H_{CH_4}, (b) H_{CO_2}, (c) $H_{C_2H_6}$, (d) $H_{C_3H_8}$, (e) $H_{C_5H_{10}}$, and (f) H_{THF}.

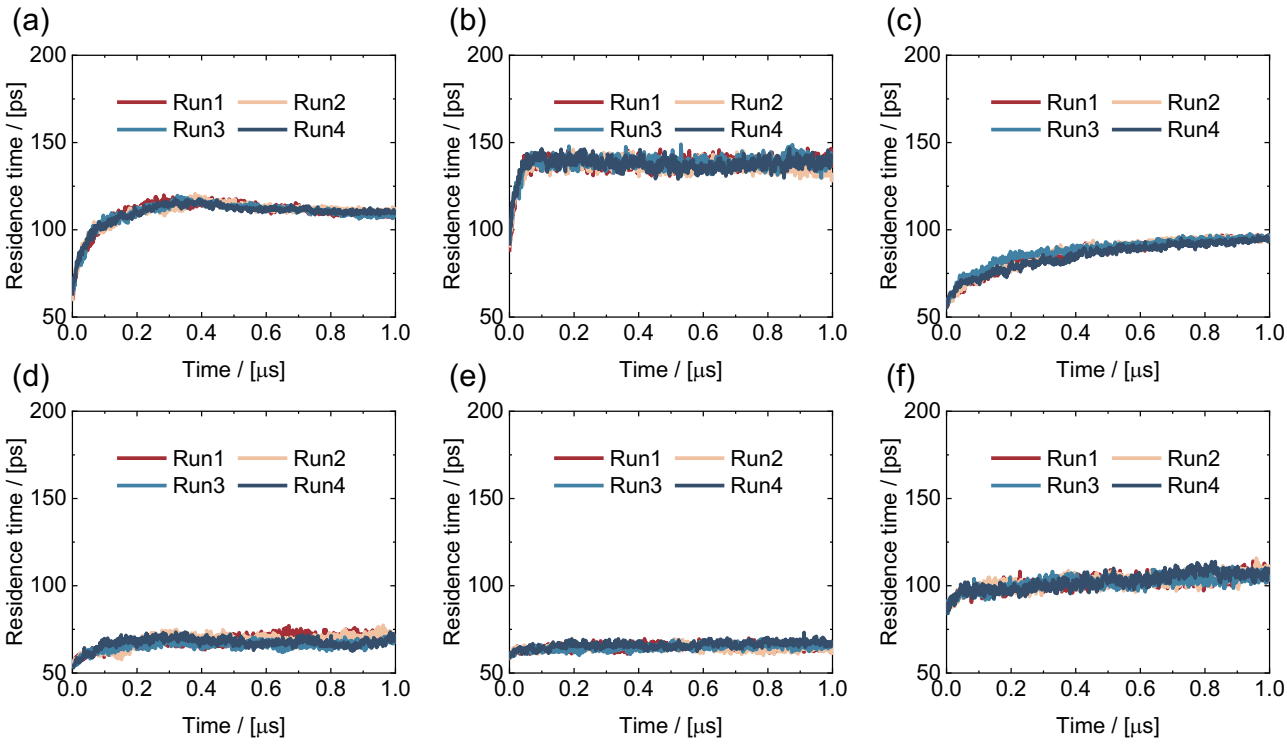

Fig. S6. Time evolution of the average residence time for H_2O molecules near promoter molecules in different repeated systems, *i.e.*, (a) H_{CH_4}, (b) H_{CO_2}, (c) $H_{C_2H_6}$, (d) $H_{C_3H_8}$, (e) $H_{C_5H_{10}}$, and (f) H_{THF}.

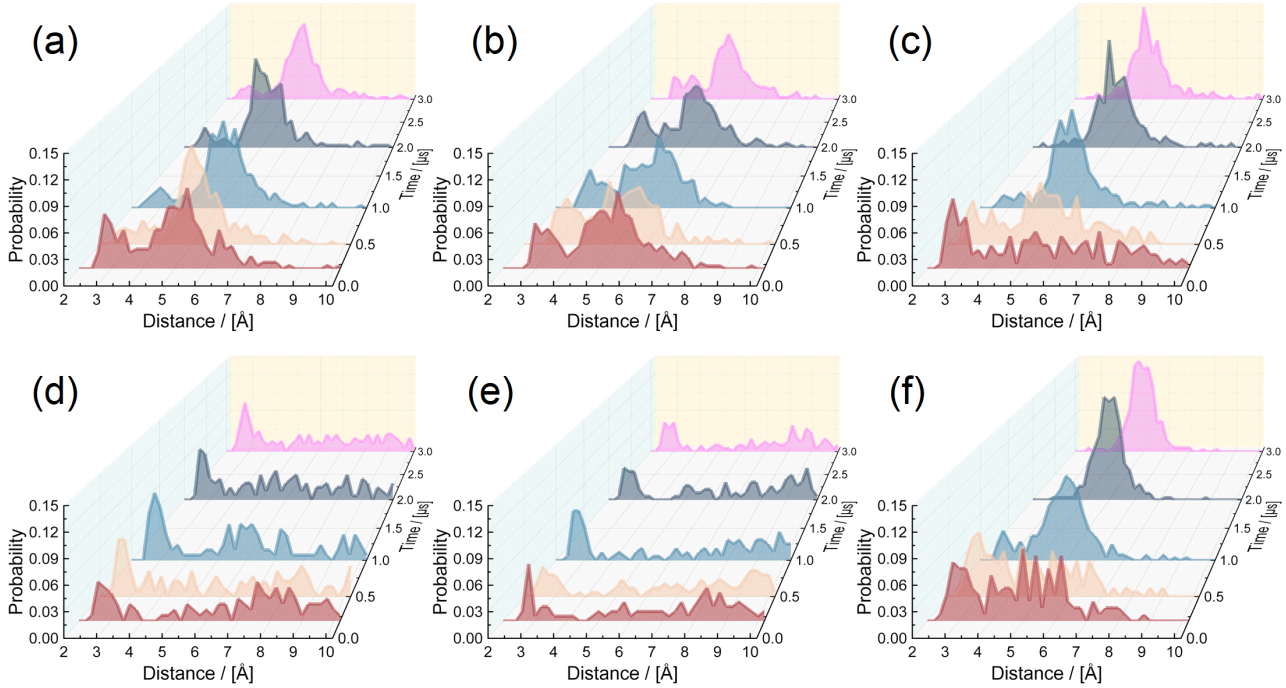

Fig. S7. Evolution of probability distribution of the distances between H_2 in water and various promoter molecules in different systems, *i.e.*, (a) H_{CH_4}, (b) H_{CO_2}, (c) $H_{C_2H_6}$, (d) $H_{C_3H_8}$, (e) $H_{C_5H_{10}}$, and (f) H_{THF}.

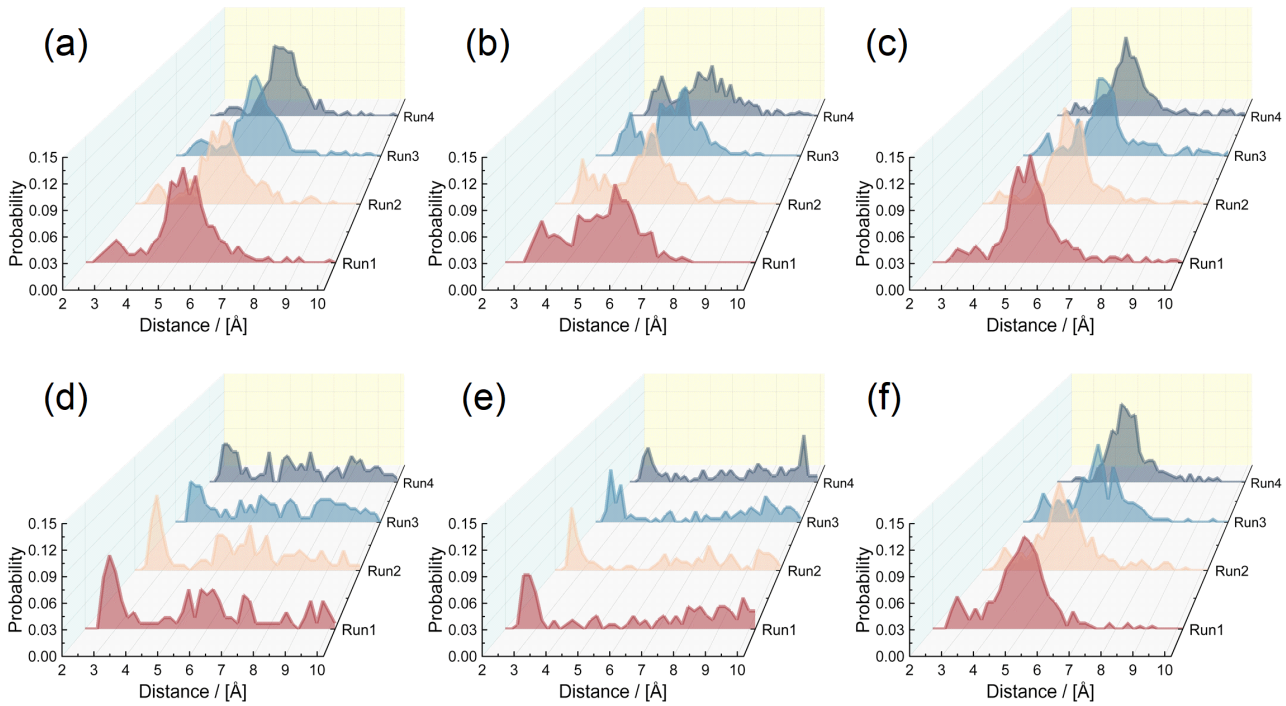

Fig. S8. Probability distribution of the distances between H_2 in water and various promoter molecules in different repeated systems, *i.e.*, (a) H_{CH_4}, (b) H_{CO_2}, (c) $H_{C_2H_6}$, (d) $H_{C_3H_8}$, (e) $H_{C_5H_{10}}$, and (f) H_{THF}.

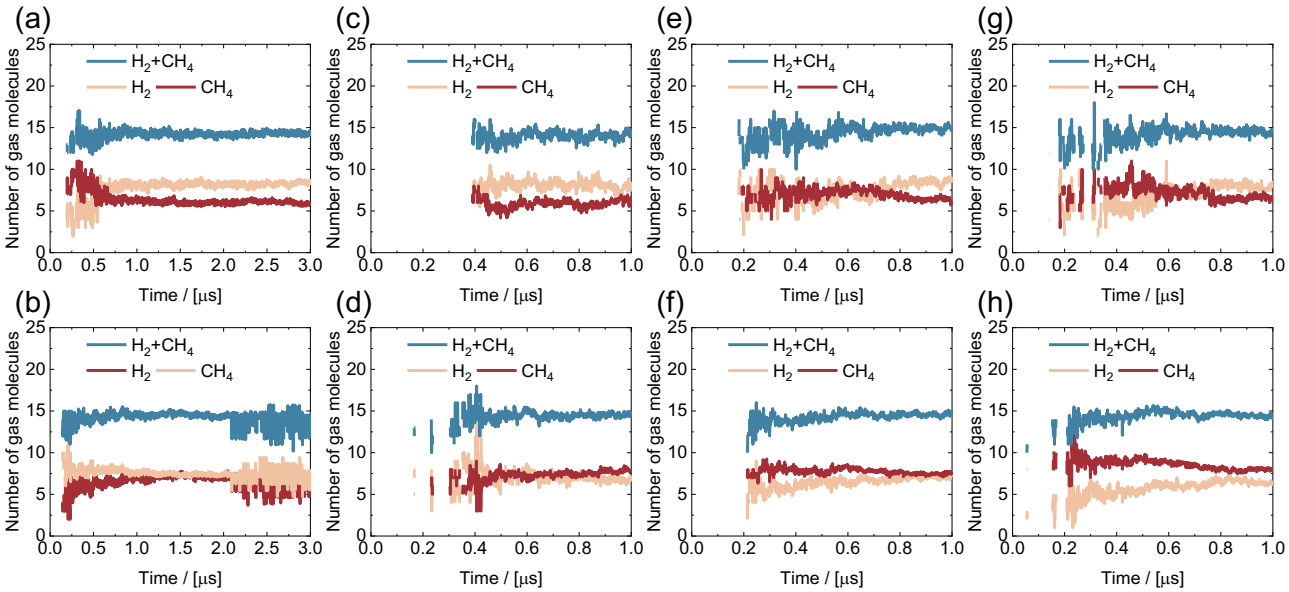

Fig. S9. Time evolution of the number of H_2 and CH_4 molecules adsorbed to each H_2-occupied and CH_4-occupied cage-faces for the H_{CH_4} repeated systems, *i.e.*, (a-b) Run1, (c-d) Run2, (e-f) Run3, and (g-h) Run4.

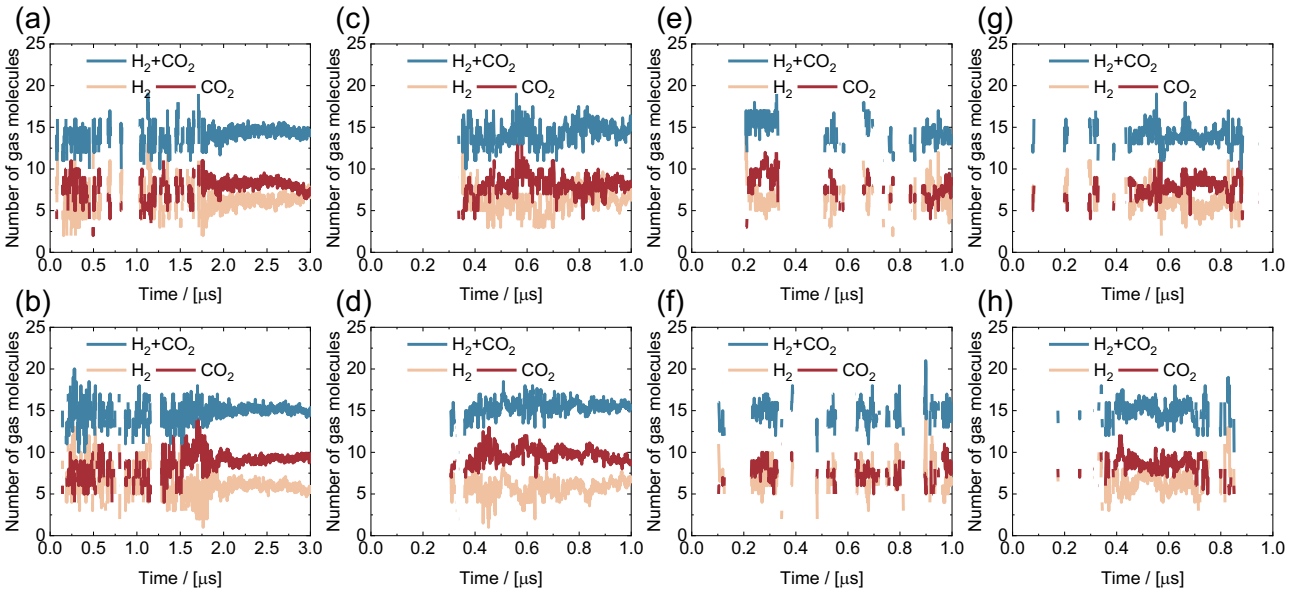

Fig. S10. Time evolution of the number of H_2 and CO_2 molecules adsorbed to each H_2-occupied and CO_2-occupied cage-faces for the H_{CO_2} repeated systems, *i.e.*, (a-b) Run1, (c-d) Run2, (e-f) Run3, and (g-h) Run4.

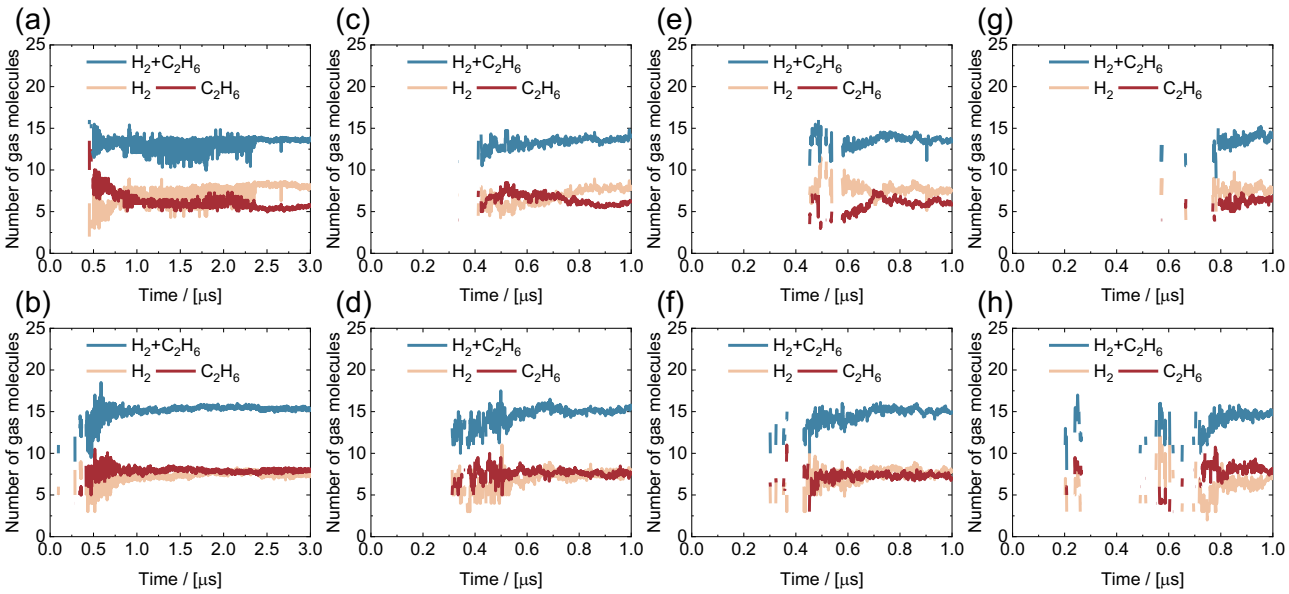

Fig. S11. Time evolution of the number of H_2 and C_2H_6 molecules adsorbed to each H_2-occupied and C_2H_6-occupied cage-faces for the $H_{C_2H_6}$ repeated systems, *i.e.*, (a-b) Run1, (c-d) Run2, (e-f) Run3, and (g-h) Run4.

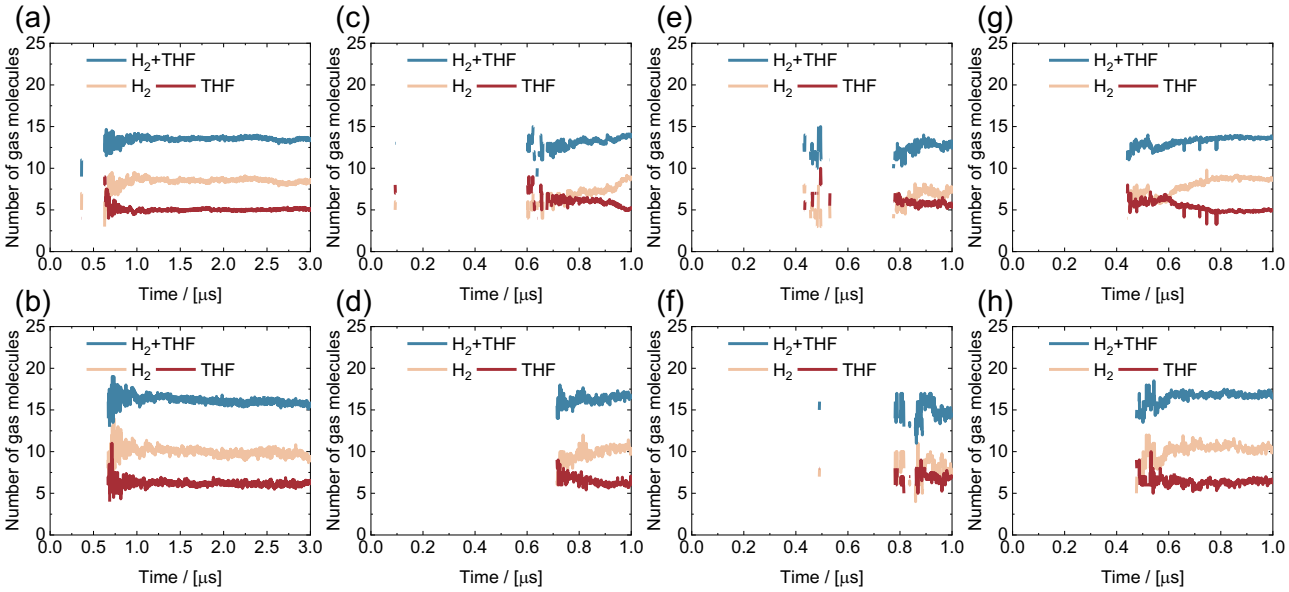

Fig. S12. Time evolution of the number of H_2 and THF molecules adsorbed to each H_2-occupied and THF-occupied cage-faces for the H_{THF} repeated systems, *i.e.*, (a-b) Run1, (c-d) Run2, (e-f) Run3, and (g-h) Run4.

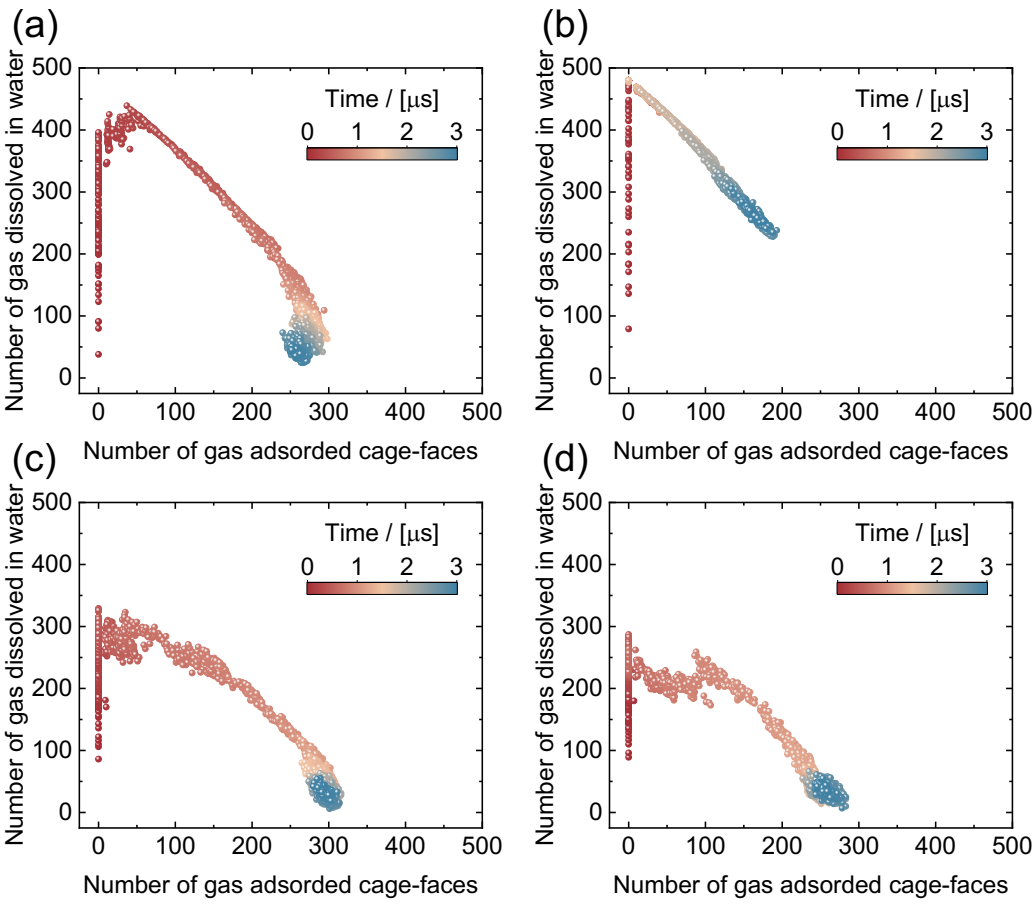

Fig. S13. Correlation plot of the number of gas molecules adsorbed cage-faces and dissolved in water for different systems, *i.e.*, (a) H_{CH_4}, (b) H_{CO_2}, (c) $H_{C_2H_6}$, and (d) H_{THF}.

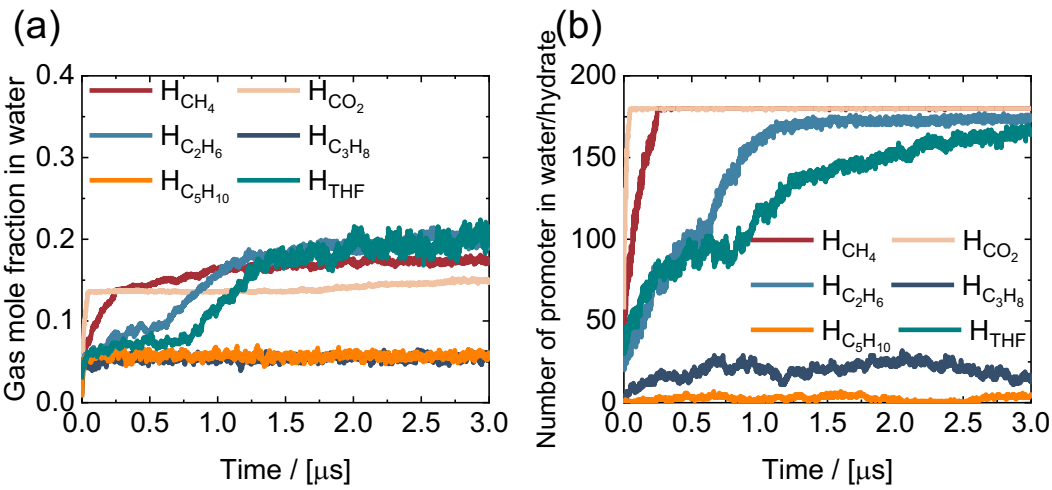

Fig. S14. Time evolution of (a) gas mole fraction x_{gas} in water and (b) the number of promoter molecules in water/hydrate for different systems, *i.e.*, H_{CH_4}, H_{CO_2}, $H_{C_2H_6}$, $H_{C_3H_8}$, $H_{C_5H_{10}}$, and H_{THF}.

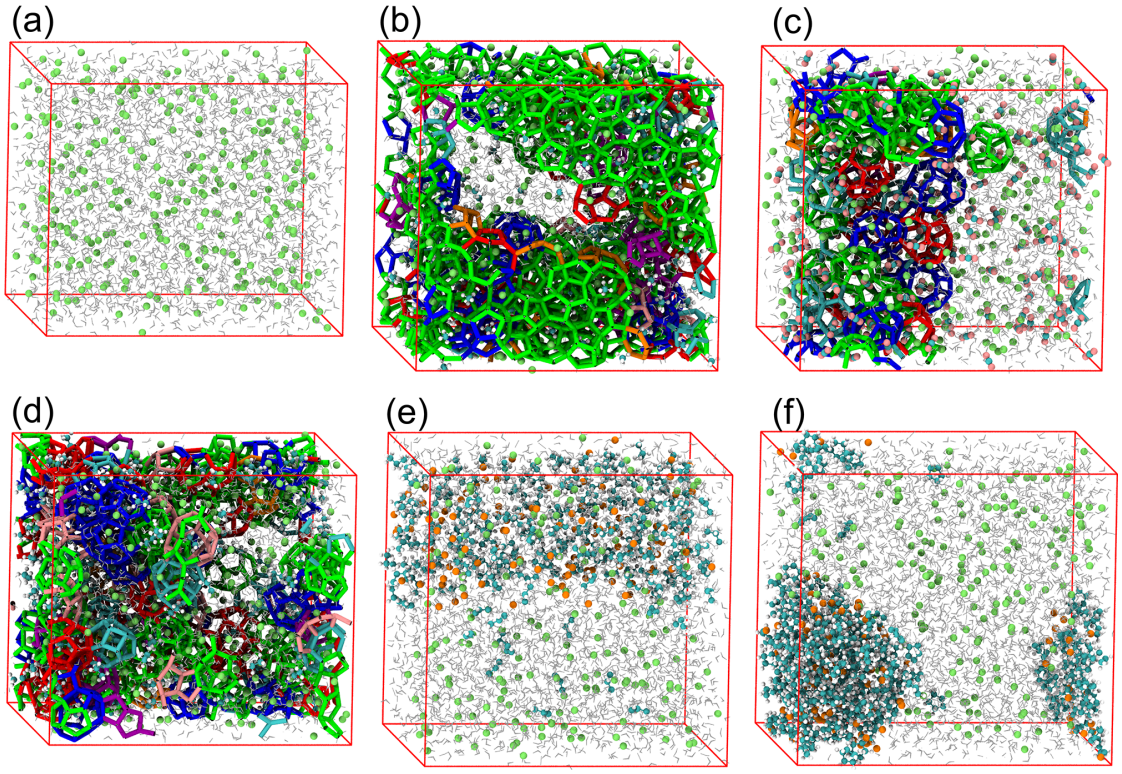

Fig. S15. Simulation snapshots of binary H_2 hydrates formed at the end of the simulation (at the 3.0 μs) in the different systems: (a) H_{Pure}, (b) H_{CH_4}, (c) H_{CO_2}, (d) $H_{C_2H_6}$, (e) $H_{C_3H_8}$, and (f) $H_{C_5H_{10}}$. Promoter molecules are displayed as cyan (C atom), red (O atom), and white (H atom). Orange balls, green balls, and silver lines represent H_2 in nanobubble, H_2 in solution, and H_2O molecules, respectively. Bonds of different colors represent seven types of hydrate cages, *i.e.*, green for 5^{12}, blue for $5^{12}6^2$, red for $5^{12}6^3$, orange for $5^{12}6^4$, cyan for $4^15^{10}6^2$, purple for $4^15^{10}6^3$, and pink for $4^15^{10}6^4$.

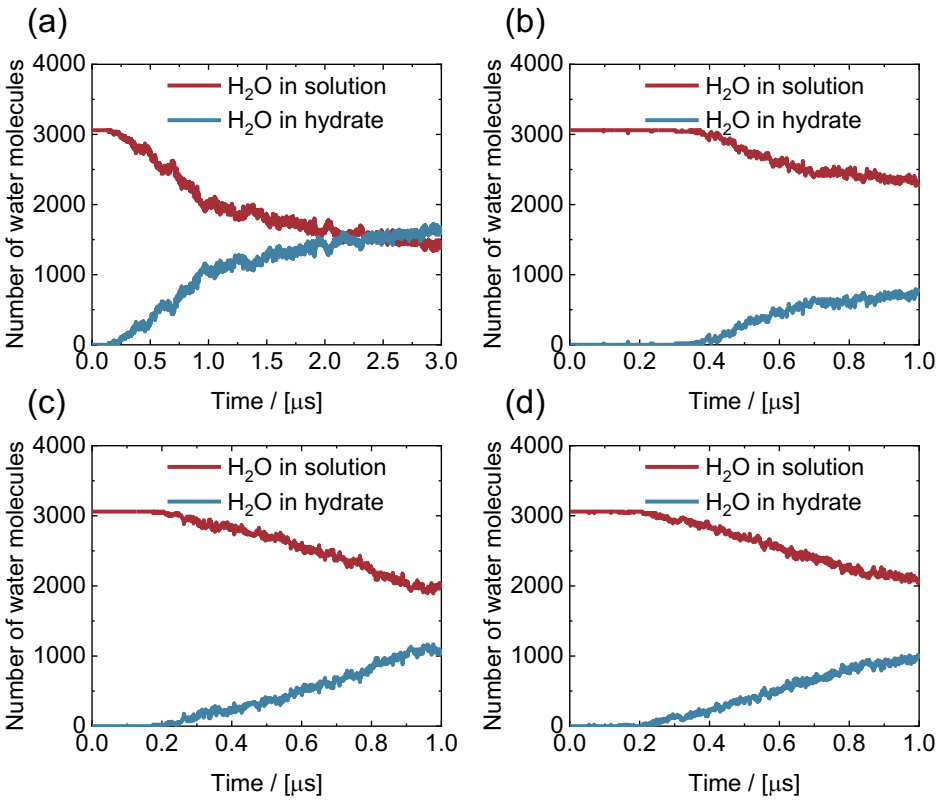

Fig. S16. Time evolution of the number of water molecules in hydrate and solution for the H_{CH_4} repeated systems, *i.e.*, (a) Run1, (b) Run2, (c) Run3, and (d) Run4.

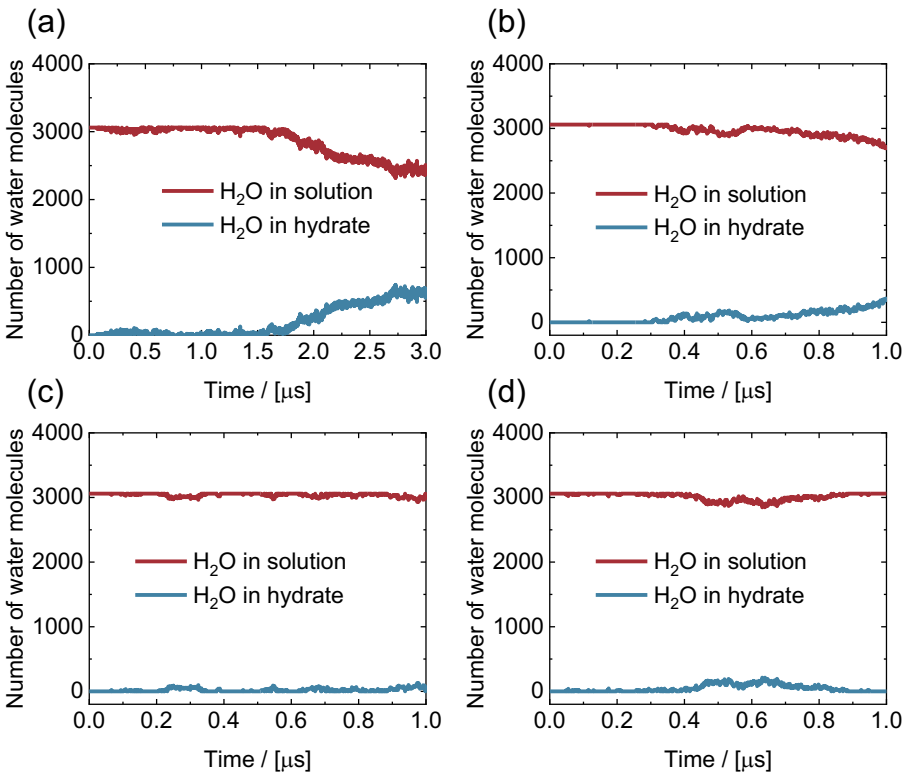

Fig. S17. Time evolution of the number of water molecules in hydrate and solution for the H_{CO_2} repeated systems, *i.e.*, (a) Run1, (b) Run2, (c) Run3, and (d) Run4.

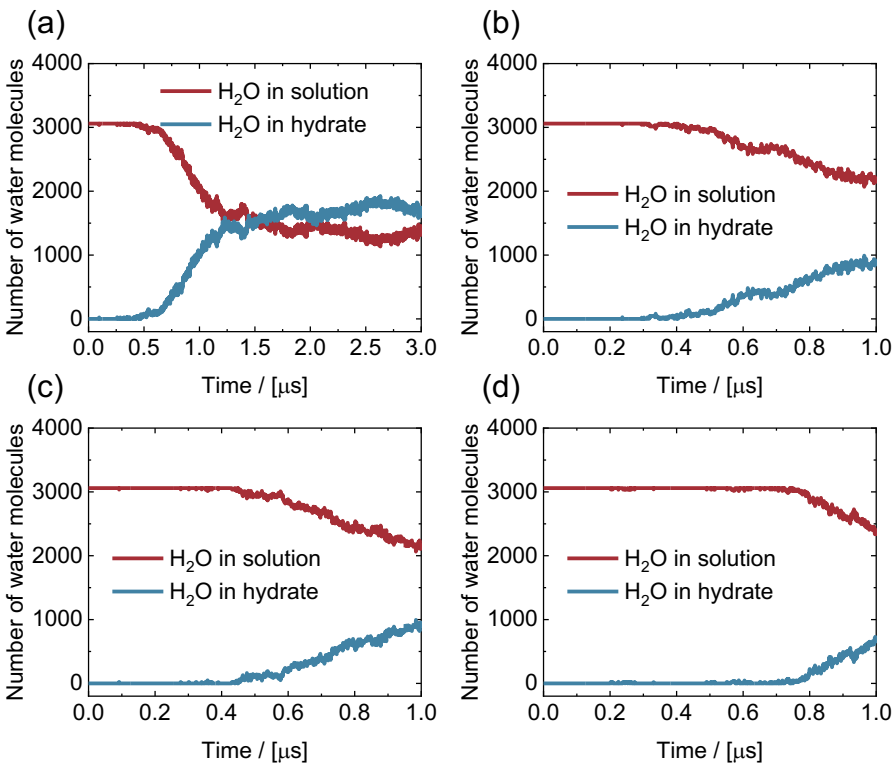

Fig. S18. Time evolution of the number of water molecules in hydrate and solution for the $H_{C_2H_6}$ repeated systems, *i.e.*, (a) Run1, (b) Run2, (c) Run3, and (d) Run4.

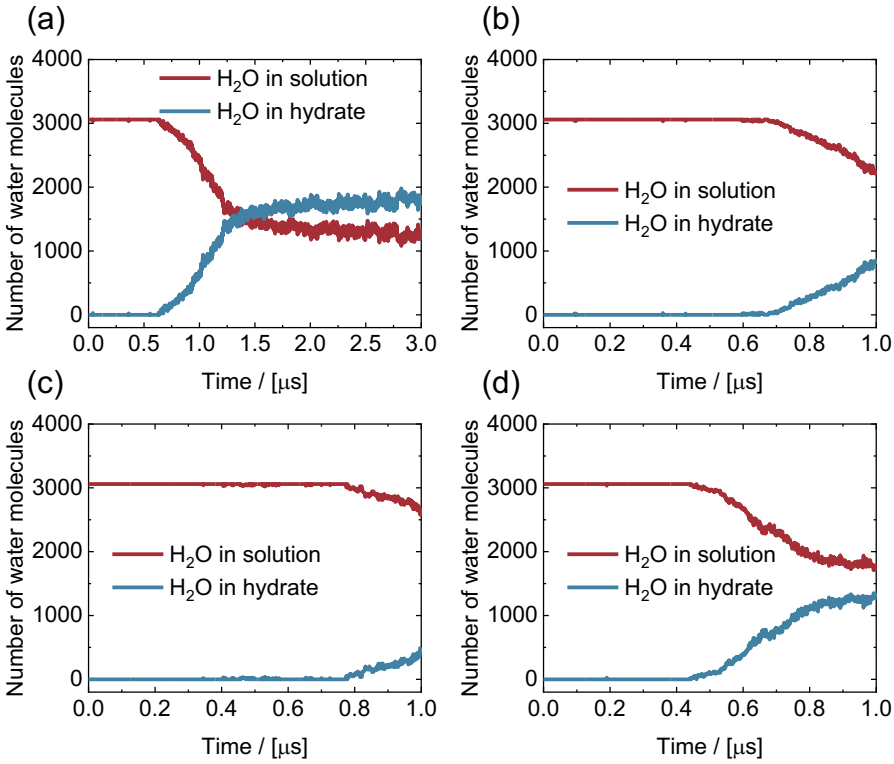

Fig. S19. Time evolution of the number of water molecules in hydrate and solution for the H_{THF} repeated systems, *i.e.*, (a) Run1, (b) Run2, (c) Run3, and (d) Run4.

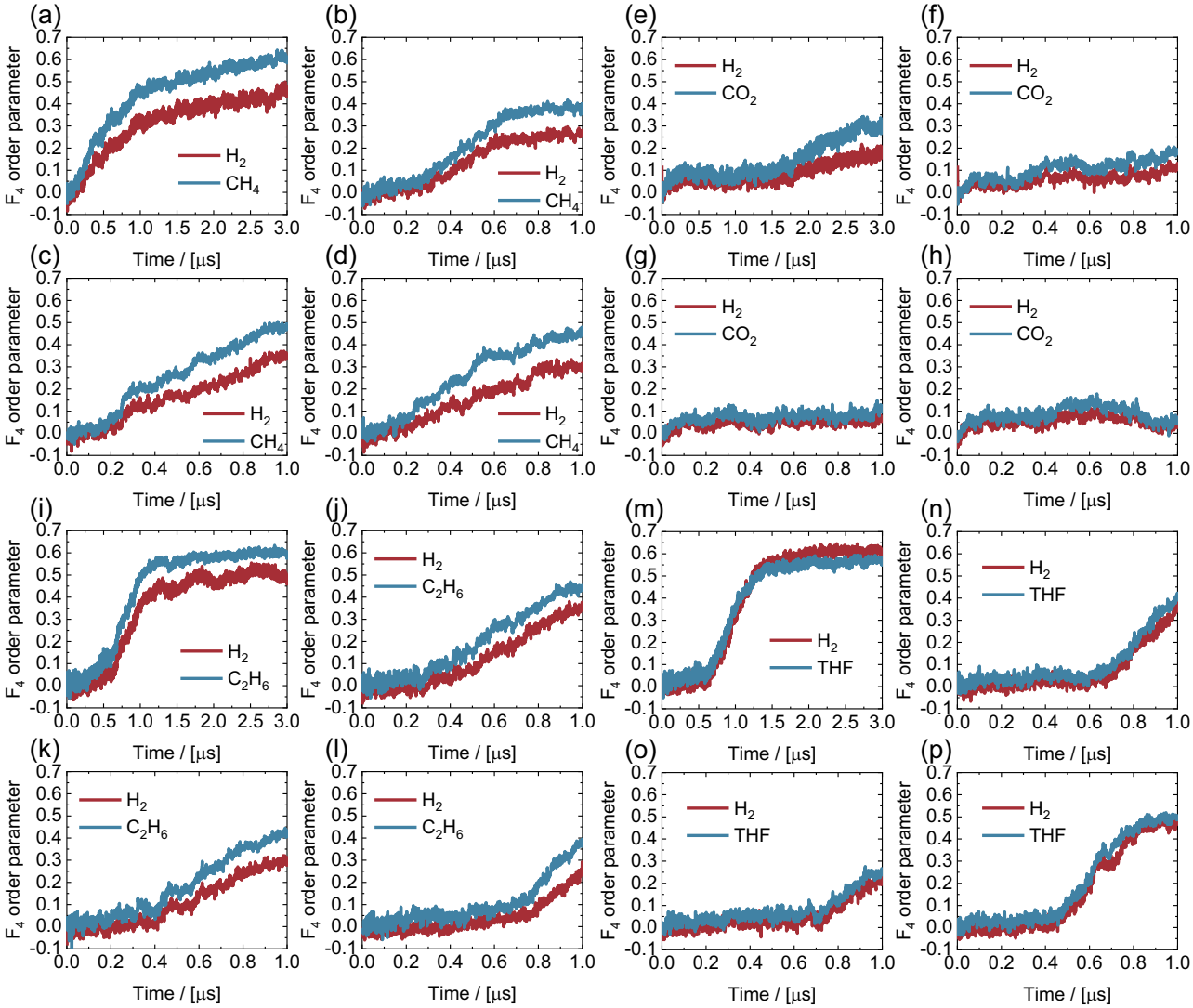

Fig. S20. Time evolution of F_4 order parameters within 0.35 nm of H_2 and promoter molecules in the four repeated simulations (Run1 - Run4) for the different systems, *i.e.*, (a-d) H_{CH_4}, (e-h) H_{CO_2}, (i-l) $H_{C_2H_6}$, and (m-p) H_{THF}, respectively.

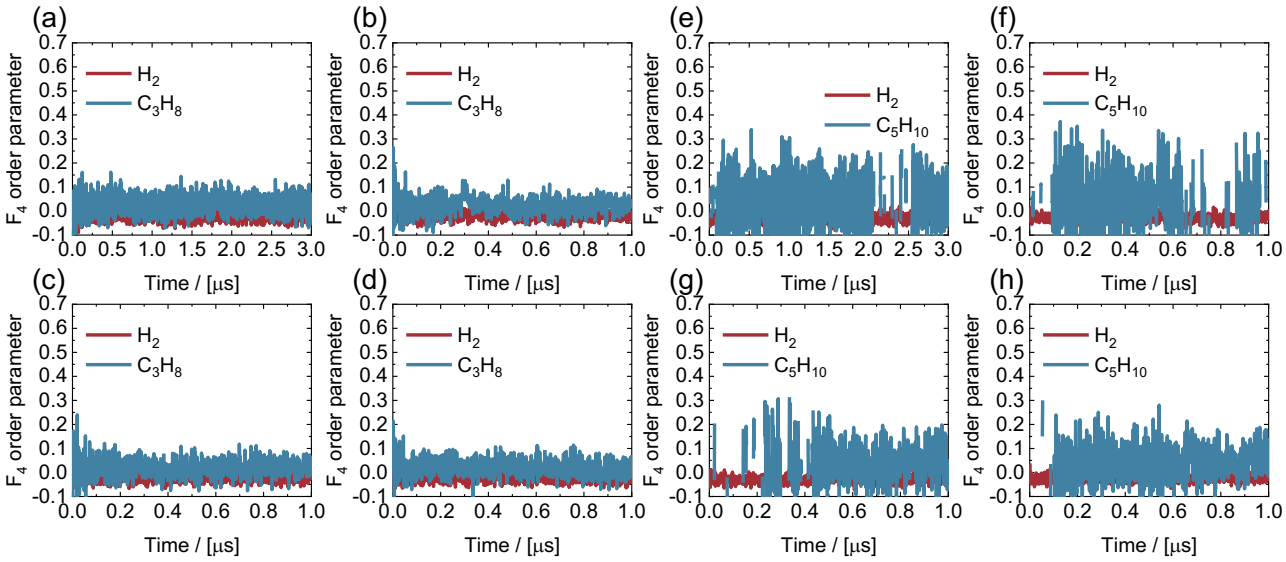

Fig. S21. Time evolution of F_4 order parameters within 0.35 nm of H_2 and promoter molecules in the four repeated simulations (Run1 - Run4) for the different systems, *i.e.*, (a-d) $H_{C_3H_8}$, and (e-h) $H_{C_5H_{10}}$, respectively.

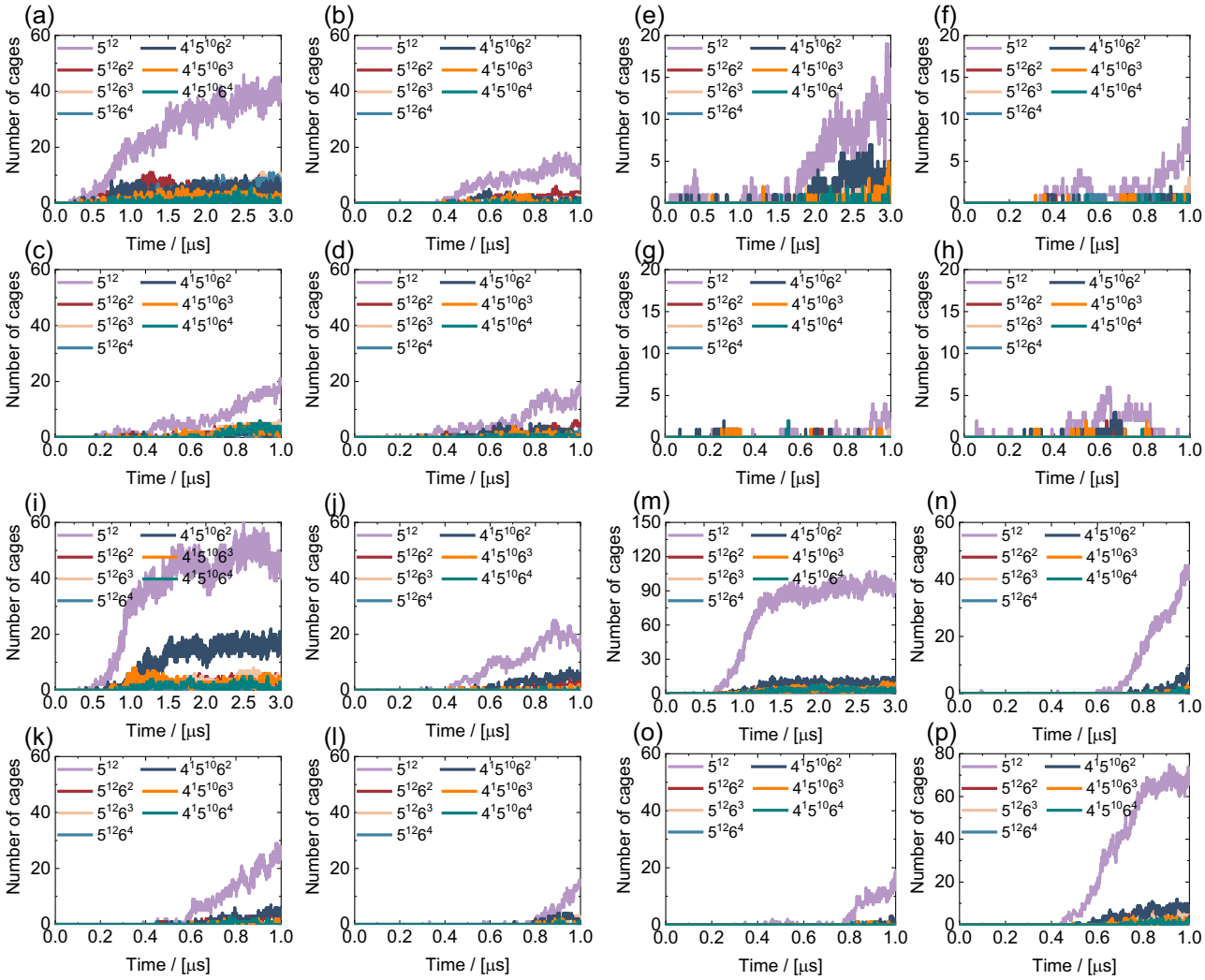

Fig. S22. Time evolution of the number of H_2-occupied cages in the four repeated simulations (Run1 - Run4) for the different systems, *i.e.*, (a-d) H_{CH_4}, (e-h) H_{CO_2}, (i-l) $H_{C_2H_6}$, and (m-p) H_{THF}, respectively.

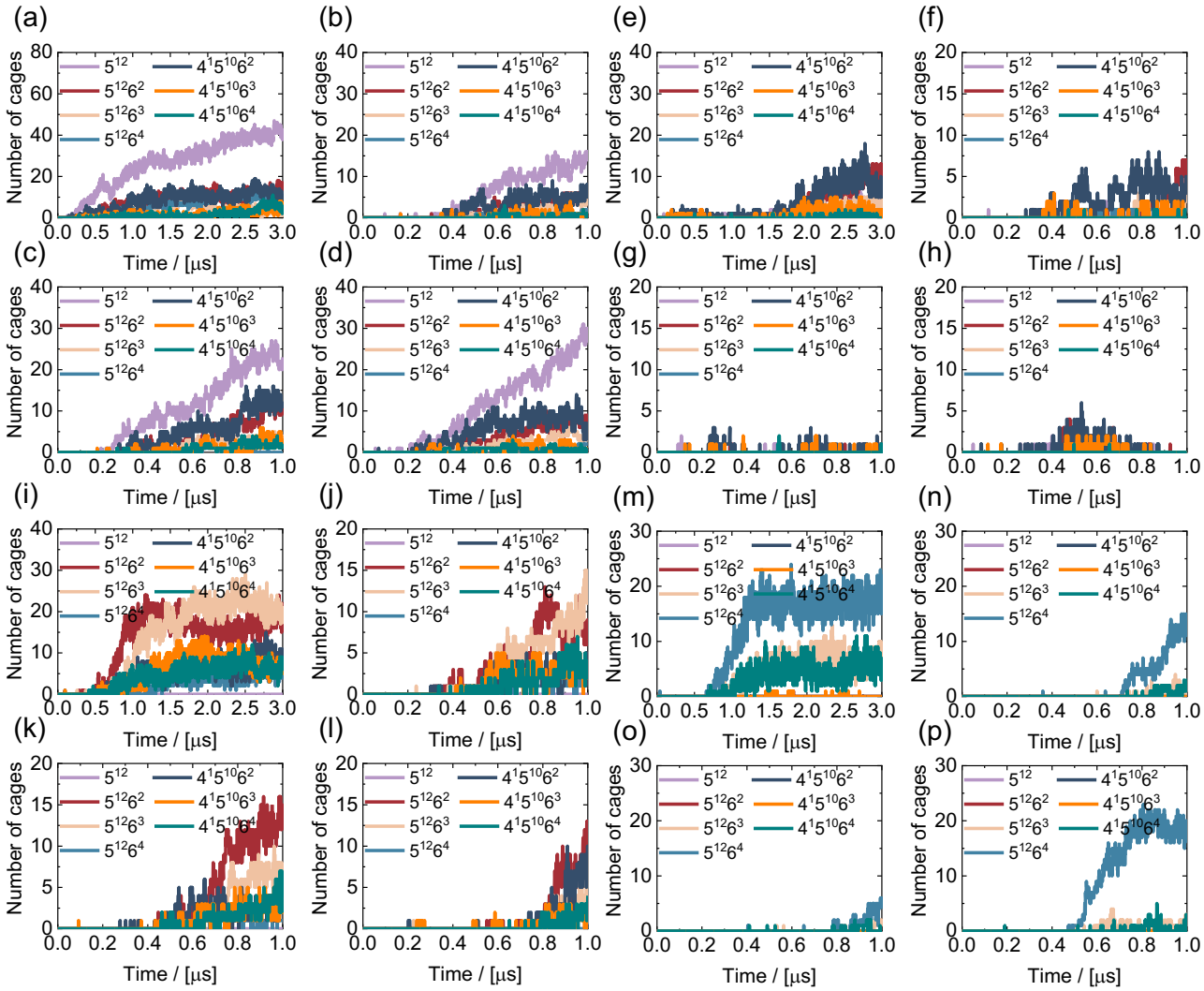

Fig. S23. Time evolution of the number of promoter-occupied cages in the four repeated simulations (Run1 - Run4) for the different systems, *i.e.*, (a-d) H_{CH_4}, (e-h) H_{CO_2}, (i-l) $H_{C_2H_6}$, and (m-p) H_{THF}, respectively.

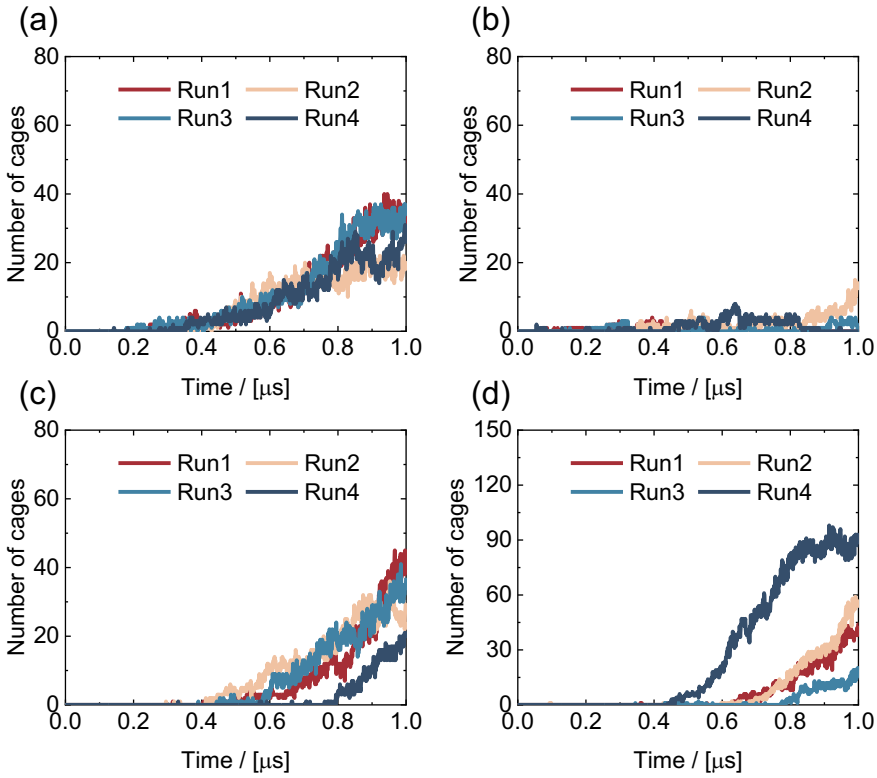

Fig. S24. Time evolution of the number of H_2-occupied cages in different systems, *i.e.*, (a) H_{CH_4}, (b) H_{CO_2}, (c) $H_{C_2H_6}$, and (d) H_{THF}.

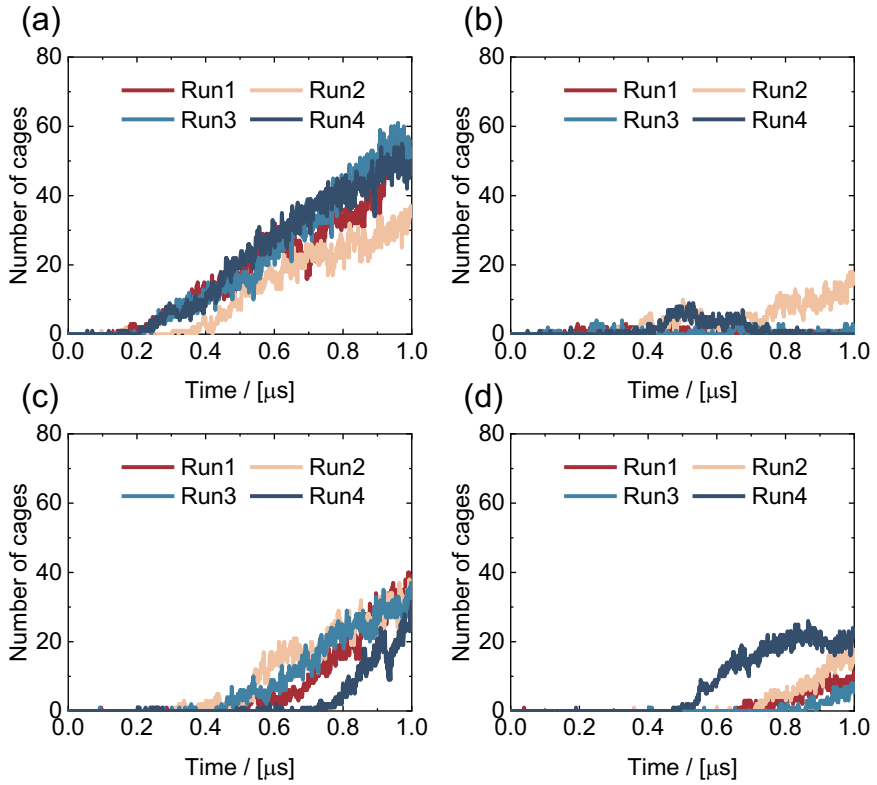

Fig. S25. Time evolution of the number of promoter-occupied cages in different systems, *i.e.*, (a) H_{CH_4}, (b) H_{CO_2}, (c) $H_{C_2H_6}$, and (d) H_{THF}.

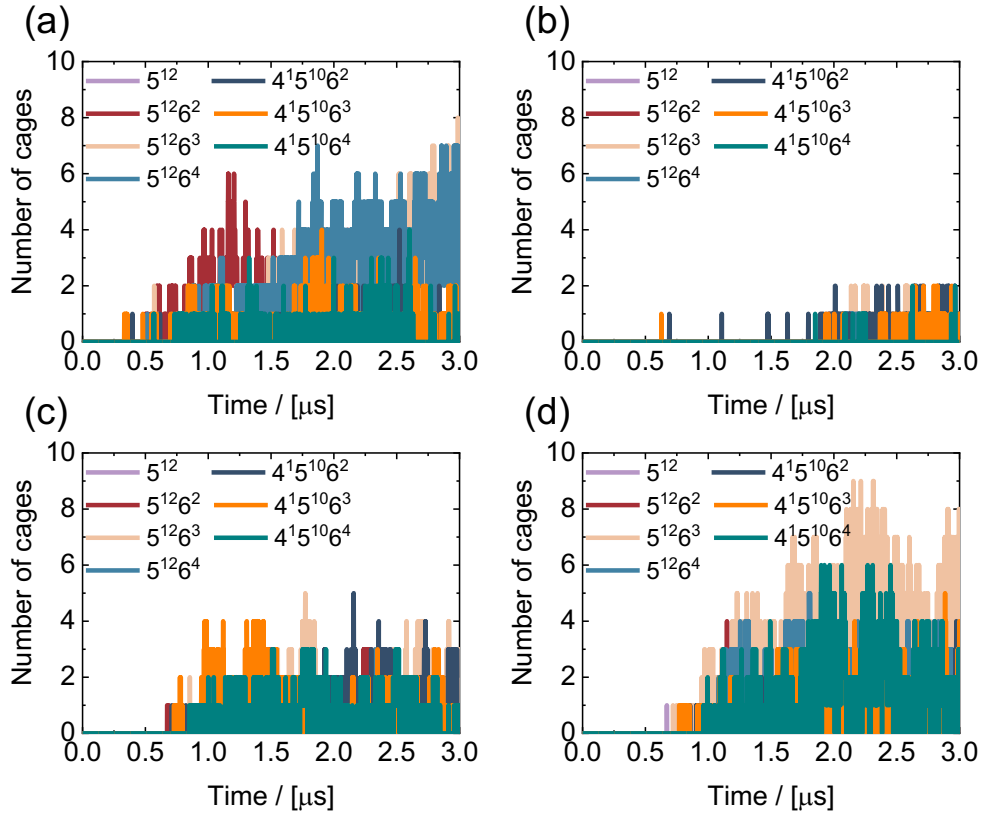

Fig. S26. Time evolution of the number of multi-occupied cages in different systems, *i.e.*, (a) H_{CH_4}, (b) H_{CO_2}, (c) $H_{C_2H_6}$, and (d) H_{THF}.

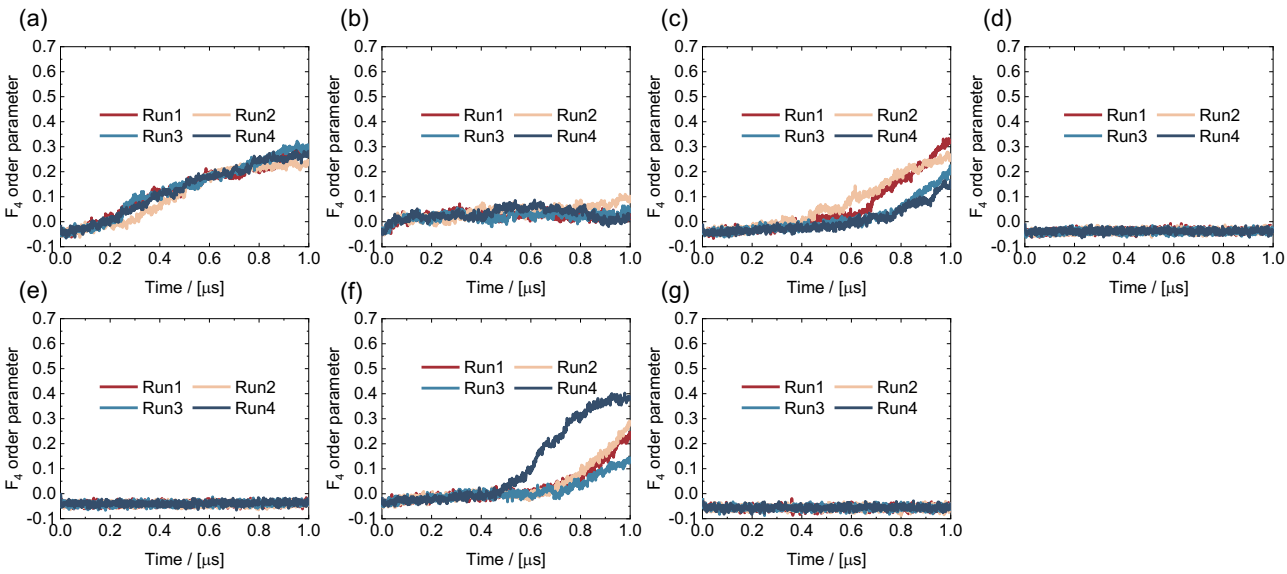

Fig. S27. Time evolution of F_4 order parameters for different systems, *i.e.*, (a) H_{CH_4}, (b) H_{CO_2}, (c) $H_{C_2H_6}$, (d) $H_{C_3H_8}$, (e) $H_{C_5H_{10}}$, (f) H_{THF}, and (g) H_{Pure}.

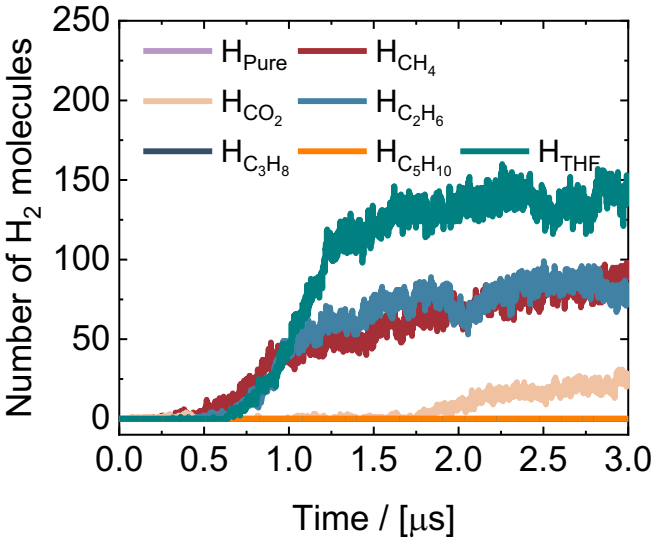

Fig. S28. Time evolution of the number of H_2 storage in hydrates for the seven systems, *i.e.*, H_{Pure}, H_{CH_4}, H_{CO_2}, $H_{C_2H_6}$, $H_{C_3H_8}$, $H_{C_5H_{10}}$, and H_{THF}.

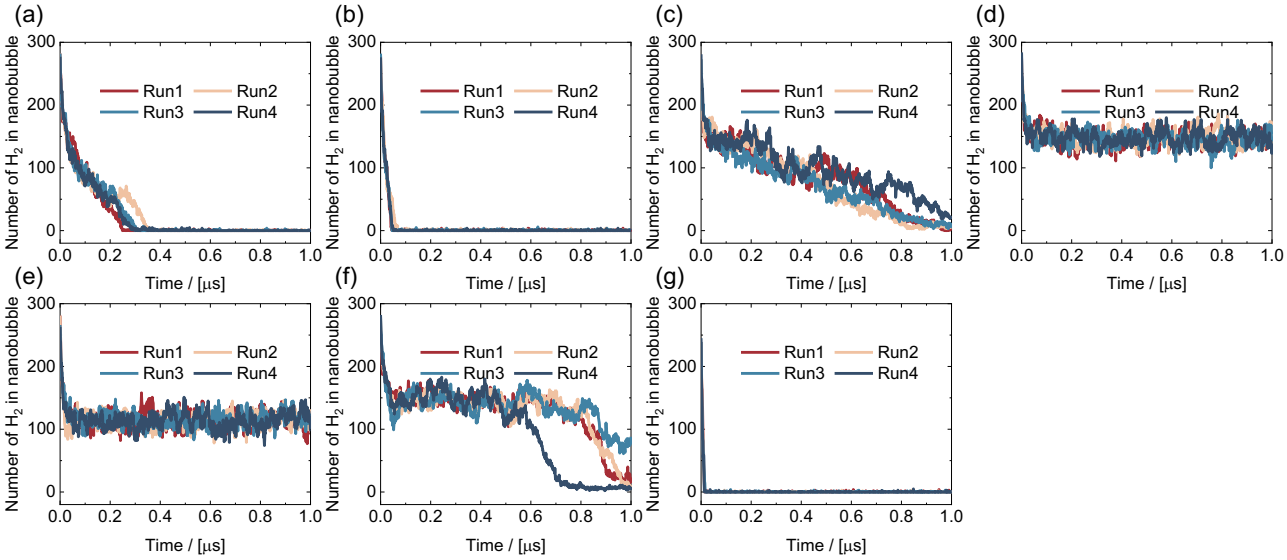

Fig. S29. Time evolution of the number of H_2 molecules in nanobubble for different systems, *i.e.*, (a) H_{CH_4}, (b) H_{CO_2}, (c) $H_{C_2H_6}$, (d) $H_{C_3H_8}$, (e) $H_{C_5H_{10}}$, (f) H_{THF}, and (g) H_{Pure}.

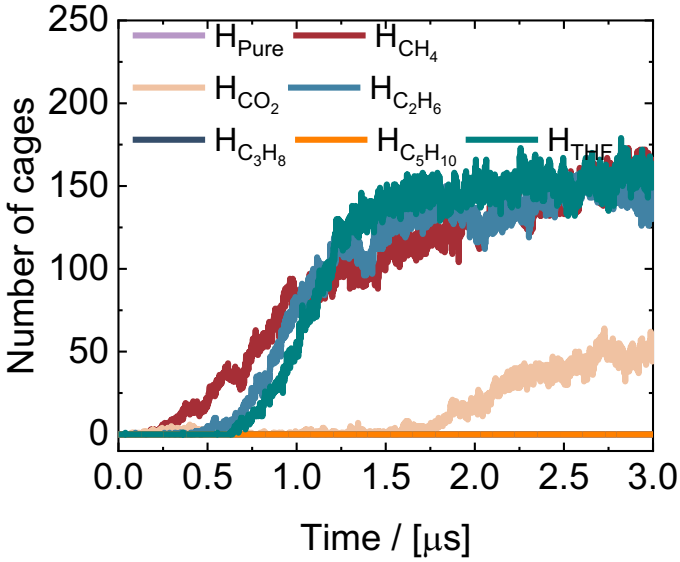

Fig. S30. Time evolution of the number of hydrate cages for the seven systems, *i.e.*, H_{Pure}, H_{CH_4}, H_{CO_2}, $H_{C_2H_6}$, $H_{C_3H_8}$, $H_{C_5H_{10}}$, and H_{THF}.

S4. Supporting Videos

Video S1. Spontaneous nucleation processes of pure H_2 hydrates from two-phase solutions for the H_{Pure} system. Green balls and silver lines represent H_2 and H_2O molecules, respectively.

Video S2. Spontaneous nucleation processes of binary H_2-CH_4 hydrates from two-phase solutions for the H_{CH_4} system. CH_4 molecules are displayed as cyan (C atom) and white (H atom). Green balls and silver lines represent H_2 and H_2O molecules, respectively. Different colored bonds represent seven types of hydrate cages, *i.e.*, green for 5^{12}, blue for $5^{12}6^2$, red for $5^{12}6^3$, orange for $5^{12}6^4$, cyan for $4^15^{10}6^2$, purple for $4^15^{10}6^3$, and pink for $4^15^{10}6^4$.

Video S3. Spontaneous nucleation processes of binary H_2-CO_2 hydrates from two-phase solutions for the H_{CO_2} system. CO_2 molecules are displayed as cyan (C atom) and red (O atom). Green balls and silver lines represent H_2 and H_2O molecules, respectively. Different colored bonds represent seven types of hydrate cages, *i.e.*, green for 5^{12}, blue for $5^{12}6^2$, red for $5^{12}6^3$, orange for $5^{12}6^4$, cyan for $4^15^{10}6^2$, purple for $4^15^{10}6^3$, and pink for $4^15^{10}6^4$.

Video S4. Spontaneous nucleation processes of binary H_2-C_2H_6 hydrates from two-phase solutions for the $H_{C_2H_6}$ system. C_2H_6 molecules are displayed as cyan (C atom) and white (H atom). Green balls and silver lines represent H_2 and H_2O molecules, respectively. Different colored bonds represent seven types of hydrate cages, *i.e.*, green for 5^{12}, blue for $5^{12}6^2$, red for $5^{12}6^3$, orange for $5^{12}6^4$, cyan for $4^15^{10}6^2$, purple for $4^15^{10}6^3$, and pink for $4^15^{10}6^4$.

Video S5. Spontaneous nucleation processes of binary H_2-C_3H_8 hydrates from two-phase solutions for the $H_{C_3H_8}$ system. C_3H_8 molecules are displayed as cyan (C atom) and white (H atom). Green balls and silver lines represent H_2 and H_2O molecules, respectively.

Video S6. Spontaneous nucleation processes of binary H_2-C_5H_{10} hydrates from two-phase solutions for the $H_{C_5H_{10}}$ system. C_5H_{10} molecules are displayed as cyan (C atom) and white (H atom). Green balls and silver lines represent H_2 and H_2O molecules, respectively.

Video S7. Spontaneous nucleation processes of binary H_2-THF hydrates from two-phase solutions for the H_{THF} system. THF molecules are displayed as cyan (C atom), red (O atom), and white (H atom). Green balls and silver lines represent H_2 and H_2O molecules, respectively. Different colored bonds represent seven types of hydrate cages, *i.e.*, green for 5^{12}, blue for $5^{12}6^2$, red for $5^{12}6^3$, orange for $5^{12}6^4$, cyan for $4^15^{10}6^2$, purple for $4^15^{10}6^3$, and pink for $4^15^{10}6^4$.

References

[1] W. Bao, Y. Teng, P. Wang, Y. Li, J. Zhu, S. Han, J. Zhu, H. Xie, Y. Zhao, Molecular analysis of hydrogen-propane hydrate formation mechanism and its influencing factors for hydrogen storage, Int. J. Hydrogen Energy 50 (2024) 697-708.

[2] F. Mi, Z. He, G. Jiang, F. Ning, What roles do interlayer cations (K+) and salt ions (Na+ and Cl−) play in methane hydrate formation in illite nanopore?, Appl. Clay Sci. 256 (2024) 107428.

[3] G. Bussi, D. Donadio, M. Parrinello, Canonical sampling through velocity rescaling, J. Chem. Phys. 126(1) (2007) 014101.

[4] H.J.C. Berendsen, J.P.M. Postma, W.F. Vangunsteren, A. Dinola, J.R. Haak, MOLECULAR-DYNAMICS WITH COUPLING TO AN EXTERNAL BATH, J. Chem. Phys. 81(8) (1984) 3684-3690.

[5] S. Nose, A Molecular-Dynamics Method for Simulations in the Canonical Ensemble, Mol. Phys. 52(2) (1984) 255-268.

[6] M. Parrinello, A. Rahman, Crystal Structure and Pair Potentials: A Molecular-Dynamics Study, Phys. Rev. Lett. 45(14) (1980) 1196-1199.

[7] T. Darden, D. York, L. Pedersen, Particle mesh Ewald: AnN·log(N) method for Ewald sums in large systems, J. Chem. Phys 98(12) (1993) 10089-10092.

[8] L.C. Jacobson, W. Hujo, V. Molinero, Thermodynamic stability and growth of guest-free clathrate hydrates: a low-density crystal phase of water, J. Phys. Chem. B 113(30) (2009) 10298-10307.

[9] J.-M. Herri, A. Bouchemoua, M. Kwaterski, A. Fezoua, Y. Ouabbas, A.J.F.P.E. Cameirão, Gas hydrate equilibria for CO2–N2 and CO2–CH4 gas mixtures—Experimental studies and thermodynamic modelling, 301(2) (2011) 171-190.

[10] H.D. Nagashima, N. Fukushima, R. Ohmura, Phase equilibrium condition measurements in carbon dioxide clathrate hydrate forming system from 199.1 K to 247.1 K, Fluid Phase Equilib. 413 (2016) 53-56.

[11] K.C. Sloan ED, Clathrate Hydrates of Natural Gases, CRC Press, Boca Raton, FL, 2008.

[12] M.M.M.-v. den Heuvel, C.J. Peters, J. de Swaan Arons, Gas hydrate phase equilibria for propane in the presence of additive components, Fluid Phase Equilib. 193(1-2) (2002) 245-259.

[13] E. Brown, M.N. Khan, D. Salmin, J. Wells, S.L. Wang, C.J. Peters, C.A. Koh, Cyclopentane hydrate cohesion measurements and phase equilibrium predictions, Journal of Natural Gas Science and Engineering 35 (2016) 1435-1440.

[14] T.A. Strobel, C.A. Koh, E.D. Sloan, Thermodynamic predictions of various tetrahydrofuran and hydrogen clathrate hydrates, Fluid Phase Equilib. 280(1-2) (2009) 61-67.

[15] J.L. Abascal, E. Sanz, R. Garcia Fernandez, C. Vega, A potential model for the study of ices and amorphous water: TIP4P/Ice, J. Chem. Phys 122(23) (2005) 234511.

[16] S. Alavi, J.A. Ripmeester, D.D. Klug, Molecular-dynamics study of structure II hydrogen clathrates, J. Chem. Phys. 123(2) (2005) 24507.

[17] J.J. Potoff, J.I. Siepmann, Vapor–liquid equilibria of mixtures containing alkanes, carbon dioxide, and nitrogen,

AlChE J. 47(7) (2001) 1676-1682.

[18] W.L. Jorgensen, D.S. Maxwell, J. TiradoRives, Development and testing of the OPLS all-atom force field on conformational energetics and properties of organic liquids, J. Am. Chem. Soc. 118(45) (1996) 11225-11236.

[19] M.J. Abraham, T. Murtola, R. Schulz, S. Páll, J.C. Smith, B. Hess, E. Lindahl, GROMACS: High performance molecular simulations through multi-level parallelism from laptops to supercomputers, SoftwareX 1 (2015) 19-25.

[20] W. Humphrey, A. Dalke, K. Schulten, VMD: visual molecular dynamics, J Mol Graph 14(1) (1996) 33-8, 27-8.

[21] L.A. Báez, P. Clancy, Computer Simulation of the Crystal Growth and Dissolution of Natural Gas Hydrates, Ann. N.Y. Acad. Sci. 715(1 Natural Gas H) (1994) 177-186.